8880

"THE EFFECT OF LOW VELOCITY IMPACT ON THE STRENGTH CHARACTERISTICS OF COMPOSITE MATERIALS LAMINATES"

End of the Year Progress Report

NASA Grant NAG 1-158

Principal Investigator: H. Liebowitz

Technical Director: E. T. Moyer, Jr.

January 7, 1986

School of Engineering and Applied Science

The George Washington University

Washington, D.C. 20052

Work under NASA Grant #NAG 1-158 has progressed significantly during the past year. The original purpose of this grant program was to investigate the nonlinear and dynamic response of composite structures to impact loading conditions. To understand this problem, it was necessary to investigate the fundamental properties of the deformation processes. To this end, the work initially focused on the response of isotropic beams subjected to pulse loading. The convergence of both finite element and finite difference solution procedures was investigated with this configuration.

Existing solutions in the literature did not model the experimentally observed behavior of impacted plates. The convergence studies demonstrated that the reason was due to the lack of an appropriate error norm. The total system energy was investigated and determined to be a good measure of accuracy. This norm was used for all further studies. The work on isotropic beam systems resulted in two publications listed as Appendixes A and B of this report.

Experimental studies were also conducted to examine the response of composite beams and plates to impact loading. The experimental work was conducted during the summer of 1984 at the Langley Research Facility under the joint direction of Dr. Wolf Elber (of NASA Langley) and Dr. E. Thomas Moyer, Jr. (of The George Washington University). These studies were carried out by Ms. Ingeresa Pincus. Here tests provided fundamental data on the indentation and flexural response of

the materials being studied in both beam and plate geometries. In addition, several fundamental properties of the deformation and onset of failure were elicited by these studies. The results of her work are presented in Appendix C.

The numerical analyses were extended to the study of circular plates subjected to impact loading. The preliminary studies involved a critical computational investigation into the behavior of the finite element method and finite difference method for solving dynamic nonlinear flexural response problems. The results indicate that the finite difference method (though rarely used in solid mechanics anymore) can be very efficient for solving nonsingular problems provided a vector computer is available (e.g., the CYBER 205). Finite element solutions also were generated. For the problems studied, both methods were comparably efficient, however, due to the simplicity of the finite difference method and the easy vectorization, it was preferable. The comparison studies were the topic of an invited conference paper included as Appendix D.

Further work was done in modeling the response to simulated impact loading through careful modeling of the momentum transfer from impactor to target. The extreme computation times required for these solutions limited the example problems which could be solved. The modeling methodology and solution procedures were, however, well tested and verified. The results of this work resulted in an invited paper presented at the ASME Winter Annual Meeting (1984) and is included as

Appendix E of this report.

To attempt to reduce the computational requirements, fundamental investigations into the convergence, stability and accuracy of several common time integrators for dynamical systems was initiated. The results demonstrated that the Runge-Kutta integrators of order four may prove to be more competitive for flexure problems than those commonly employed (e.g., central difference method, Newmark's method, etc.). Preliminary results were presented at the SES Annual Meeting (October, 1985) and will be the topic of a future NASA contractor report and publication. The results presented at the meeting are summarized in Appendix F.

During the summer of 1985, the focus of the research changed to investigate the response of plates to acoustic loading. Preliminary unpublished experiments from the NASA Langley Reseach Center demonstrated that the response of many panels relevant to application exhibited significant nonlinear characteristics. The solution methodology developed for the impact simulations provides the basic tools necessary to address these problems. Our most recent work is focusing on the development of accurate and efficient solutions to acoustic response of plates. The formulation of the fundamental equations and the specific problems being investigated are presented fully in the project proposal.

A computer program for the solution of circular plate problems has been developed and is under testing. The program

can analyze arbitrary loading and damping properties. Finite difference operators have been employed for spatial discretization. Different time integrators are being utilized as necessary as the damping terms introduce different convergence properties than exhibited by the undamped system.

In addition to the work cited above, further research has been done in the convergence properties of finite elements for solving many types of nonlinear vibration problems. This work has delineated the grid requirements, time step requirements and error norm magnitudes necessary for accurate solutions to be generated. This work was performed by a candidate (Mr. E. Ghashghai-Abdi) for the Master of Science degree at The George Washington University and is the subject of his thesis (in progress). This work will be the subject of a NASA contractor report at its completion.

The work under NASA Grant NAG #1-158 has produced many important results summarized above and detailed in the Appendices. In addition, the computational approaches developed for solving impact problems are largely applicable to acoustic problems. The extension into this domain was natural and is the subject of our current work. The investigators wish to thank Dr. Wolf Elber (Technical Monitor of this Grant) for his continual support, encouragement and involvement in this research.

APPENDICES

APPENDIX C:

"Low-Velocity Impact Tests and Static Indentation Tests Conducted to Determine Strain Behavior on Composite Plates Test Procedures and Results."

By: Ingeresa T. Pincus.

Low-Velocity Impact Tests and Static Indentation Tests Conducted to Determine Strain Behavior on Composite Plates

Test Procedures and Results

Inger T. Pincus
August 17,1984

SUMMARY

Static indentation tests were performed on 8-ply quasi-isotropic graphite/epoxy composite materials to serve as a basis of comparison to dynamic tests.

Low velocity impact tests were conducted with the same materials to provide supporting data for theoretical analysis developed by Dr. Thomas Moyer. Strain was recorded for several locations on both circular and beam-shaped specimens. Strain versus time graphs were then plotted for impacts of various magnitude.

The results demonstrated that the strain behavior was a function of position along the radius and dependent upon the flexure and membrane behavior of the material.

INTRODUCTION

The increasing use of composite materials in aircraft structures necessitates research into deformation and failure patterns. Determining damage from low velocity impacts is of great importance because the occurrence of this type of impact is highly possible. In addition, resulting damage which could propagate through the material may not be visible on the surface.

The purpose of this report is to explain the static indentation and low-velocity impact tests conducted on composite materials. The report will include a description of the test set-ups and procedures and and a graphical presentation of the test results.

EXPERIMENTAL PROCEDURES

Materials

Two 8-ply quasi-isotropic composite materials of graphite in Narmco 5208 epoxy resin (T300/5208) were tested. Material A was a woven fabric laminate and Material B was a tape laminate. Specific material properties are listed in Table 1.

Static Tests

Static indentation tests were conducted first. These tests, described briefly below, generated load versus displacement curves and strain versus displacement curves.

Test Set-up

The composite materials were cut into 7" squares and 1"x7" beams and bonded with epoxy to square aluminum plates with 5" diameter apertures. The specimens were clamped to a test stand mounted onto the hydraulic ram of an MTS servo-hydraulic test machine. The indenter, a cylinder with a 1" steel ball attached to the tip was mounted to a load cell from above. Two DCDT displacement gauges attached to the sides of the indenter measured the displacement of the plate under loading. This set-up is shown in Photos Nos. 1 and 2.

Test Procedure and Analysis

During one static indentation test cycle, the displacement followed a triangular waveform with a set maximum. The resulting load applied to the specimen during the test was recorded. (The calibration of the displacement gauges was 1 volt = 0.6312 mm. and the span of the machine ranged from 0 to 10 volts.) The load versus displacement curves generated for the two materials are shown in Figures 1 and 2.

According to the analysis developed by Dr. Wolf Elber and Gretchen Bostaph in Ref. 1, the reaction of a plate to a load is determined by the combination of plate shear and flexural stiffness, together with membrane extensional stiffness. The theory predicts that large diameter plates, such as the test specimens used, would be dominated by the membrane behavior. The analytical load versus displacement curve for a membrane-dominated plate, presented in Ref. 1, has an initial continuous, nonlinear slope as did the curves in Figs. 1 and 2. Comparatively, the typical curve for a small diameter plate, where the flexural behavior dominates, has an initial linear slope followed by a sudden drop, indicating the onset of delamination.

Strain gauges were mounted at several locations along the radius of the plate and measured during small displacements of the plate. Strains were plotted against displacement, demonstrating changes due to flexural and membrane strains. Figures 3 to 8 demonstrate strains on a circular plate and Figures 7 and 8 show the strains on a fixed beam. As predicted in Ref. 1, the flexural strains were tensile inside the inflection point and compressive outside, for the bottom surface. Strains on the top surface were opposite in sign. The overall strain behavior, however, was also influenced by membrane tension. The dominating contribution of membrane strains was exhibited by the graphite epoxy material, shown in Figure 5.

The indentation of the plate, caused by the indenter, contributes to the total displacement of the plate. As explained in Ref. 1, a function representing this indentation is determined from the load versus displacement curves of specimens totally supported underneath. Unlike the other static indentation tests, the machine was set on load control and the displacement

recorded. (One volt corresponded to 400 pounds of load.) These indentation functions (representing the load versus displacement curves shown in Figures 9 and 10) were calculated by transforming the data into linearized form and performing linear regression. The linearized data and the best line fit is shown in the Appendix.

Low Velocity Impact Tests

Test Specimens

Two types of specimens were tested: 5" diameter circular plates, similar to the status test specimens, and beam plates 1"x5", fixed on the ends. Eight strain gauges were bonded to each specimen in specific locations with respect to the point of inflection. Strain is initially zero at the inflection point for a plate subject to a center unit load. The exact location was calculated from the following equation for deflection of a circular plate with clamped edges, loaded at the center:

$$W = \frac{Pr^2 \log r/a}{8\pi D} + \frac{P(a^2-r^2)}{16\pi D}$$

where "a" is the radius of the plate, and "r" is the distance from the center.

The second derivative with respect to "r" is:

$$\frac{d^2w}{dr^2} = \frac{P}{4\pi D} [1+\log r/a]$$

From this equation the location of the inflection point was obtained.

$$\ln r = -1 + \ln a$$

$$r/a = e^{-1} = 0.37$$

As shown, the point of inflection was located at a distance $r = 0.37a$ from the center. Strain readings were desired at this point in order to record the fluctuations in strains due to the combined effect of the

membrane and flexural strains. Strains were also recorded at a distance r = 0.75a where the strain behavior was less sensitive to position. In order to observe differences between strains oriented along the direction of the fibers (0° direction) and strains oriented at 90° from the direction of the fibers, gauges were placed in both directions on the circular plates. The exact locations and labels for the strain gauges bonded on the 127 mm. circular plate were the following:

- Strains A & B: r = 23.5 mm., top and bottom surface
- Strains C & D: r = 47.6 mm., top and bottom surface

Strains A through D were all oriented in the 0° direction on the circular plates and in the 45° direction on the beam plates.

Strains 1 through 4 corresponded to the same locations as A through D, except that they were oriented in the 90° direction.

Test Procedure

The device used to produce the impact consisted of a 1" diameter steel ball attached to the end of a fiberglass cantilever. Mounted on top of the ball was an accelerometer to measure the vibration of the plate. The specimen was placed in a position so that the cantilever rested horizontally and unstressed when the ball contacted the center of the specimen. This test set-up can be seen in Photos Nos. 3 and 4. To produce the impact, the cantilever and ball were lifted to a specific height and dropped. The release heights covered the range of 1" to 8" in one-inch increments. Each height corresponded to a specific maximum load to which the plate was subjected. The equation for this "max" load was derived by representing the cantilever as a simple harmonic spring and determining the acceleration in terms of the duration of the impact. This max load is:

$$P_{max} = \frac{-\pi V_o M}{T}$$

Where "M" is the mass of the ball and cantilever, "T" is the duration of the impact, and "Vo" is the velocity of the ball when it strikes the plate, which is represented by the equation:

$$Vo = \sqrt{\frac{Kh^2}{M} + 2gh}$$

where "K" is the stiffness constant for the cantilever and "h" is the release height. The constants used for analysis are found in Table 1.

DATA

Strains were read and recorded on a four channel Nicolet Oscilloscope. The strain gauges used had a gauge factor of 2.0±0.1 and a resistance of 120 ohms. The output was measured and amplified through a Bridge Amplifier and Meter (BAM-1) and calibrated for 1 volt equal to 4000 $\mu\epsilon$. These voltage readings were recorded on Channels 1A and 2A of the oscilloscope. The time duration of the impact was recorded on Channel 2B and the acceleration on Channel 1B. The equipment used can be seen on Photo No. 5.

ANALYSIS

The information recorded on the four channels of the oscilloscope was originally stored on a magnetic disk. During the test, readings were taken every two milliseconds, producing an extremely large number of data points. The data was fed through a program designed to reduce the number of data points to below 200. The new data set was then stored on magnetic tapes. The strain readings were then converted from volts to microstrains by a calibration program. Strain versus time curves were plotted to display the test results in useful form.

RESULTS

The results of the low velocity impact tests are shown in Figures 11 through 16. The strains measured for each impact were plotted according to the location of the strain measurement. The different curves represent the increasing release heights for the impacts, producing increasing loads on the specimens.

The graphs indicated that the duration of impact decreased as the "max" load of impact increased. The larger impacts caused an increase in strain magnitude. However, the pattern of strain behavior remained very similar in most cases. The large contribution of membrane tension in the graphite epoxy composite is illustrated in the dynamic test curves by the tendency towards positive total strain at locations of compressive flexural strain.

The results of the beam specimen differ from those of the circular plate specimens primarily in the magnitude of the strains. The beams respond with higher strains and also illustrate more flexural characteristics.

CONCLUDING REMARKS

An 8-ply graphite epoxy composite material and an 8-ply woven fabric composite material were chosen for testing. The materials were cut into 5" circular plates and 5"x1" beams.

The following tests were conducted:

1. Static indentation: From these tests, load versus displacement curves and strain versus displacement curves were generated.

2. Indentation on fully backed specimens: These tests produced the indentation functions for the two materials.
3. Low-velocity impact: These tests provided the strain behavior data needed to support theoretical analysis developed by Dr. Thomas Moyer.

[HP2]

REFERENCES

1. Bostaph,Gretchen M.;and Elber,Wolf,Static Indentation Tests on Composite Plates for Impact Susceptibility Evaluation. Proceedings of the Army Symposium of Solid Mechanics, 1982-Critical Mechanics Problems in Systems Design,AMMRC MS 82-4, U.S. Army,Sept. 1982,pp. 288-317.

2. Bostaph,Gretchen M.;and Elber,Wolf, A Fracture Mechanics Analysis for Delamination Growth During Impact on Composite Plates.

3. Elber,Wolf, Failure Mechanics in Low-Velocity Impacts on Thin Composite Plates.NASA TP 2152,1983.

4. Timoshenko,S.;and Woinowsky-Krieger,S., Theory of Plates and Shells, McGraw-Hill Book Company,New York,1959,pp.51-78.

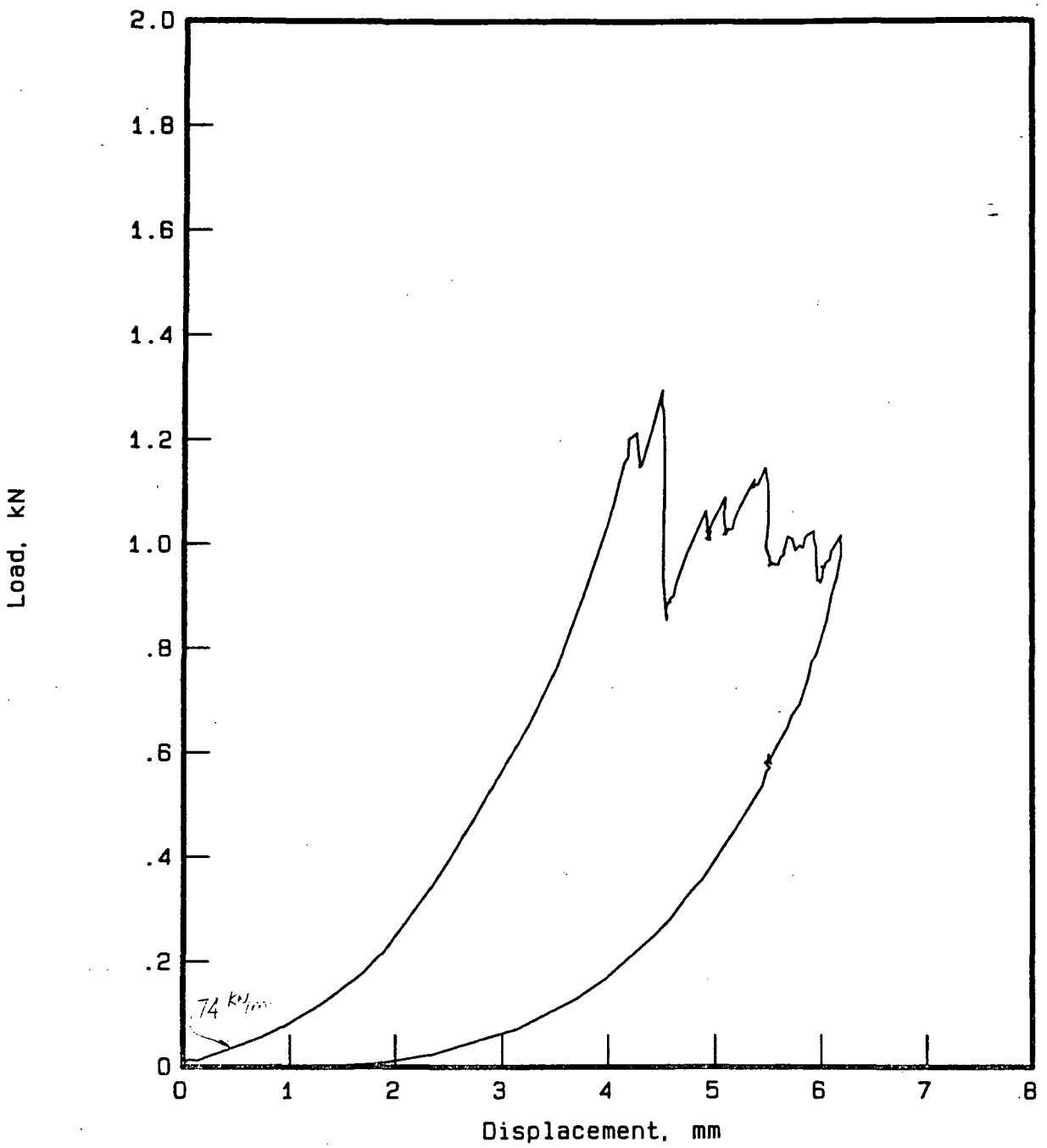

Fig. 1 - Load vs. Displacement Curve for woven fabric material

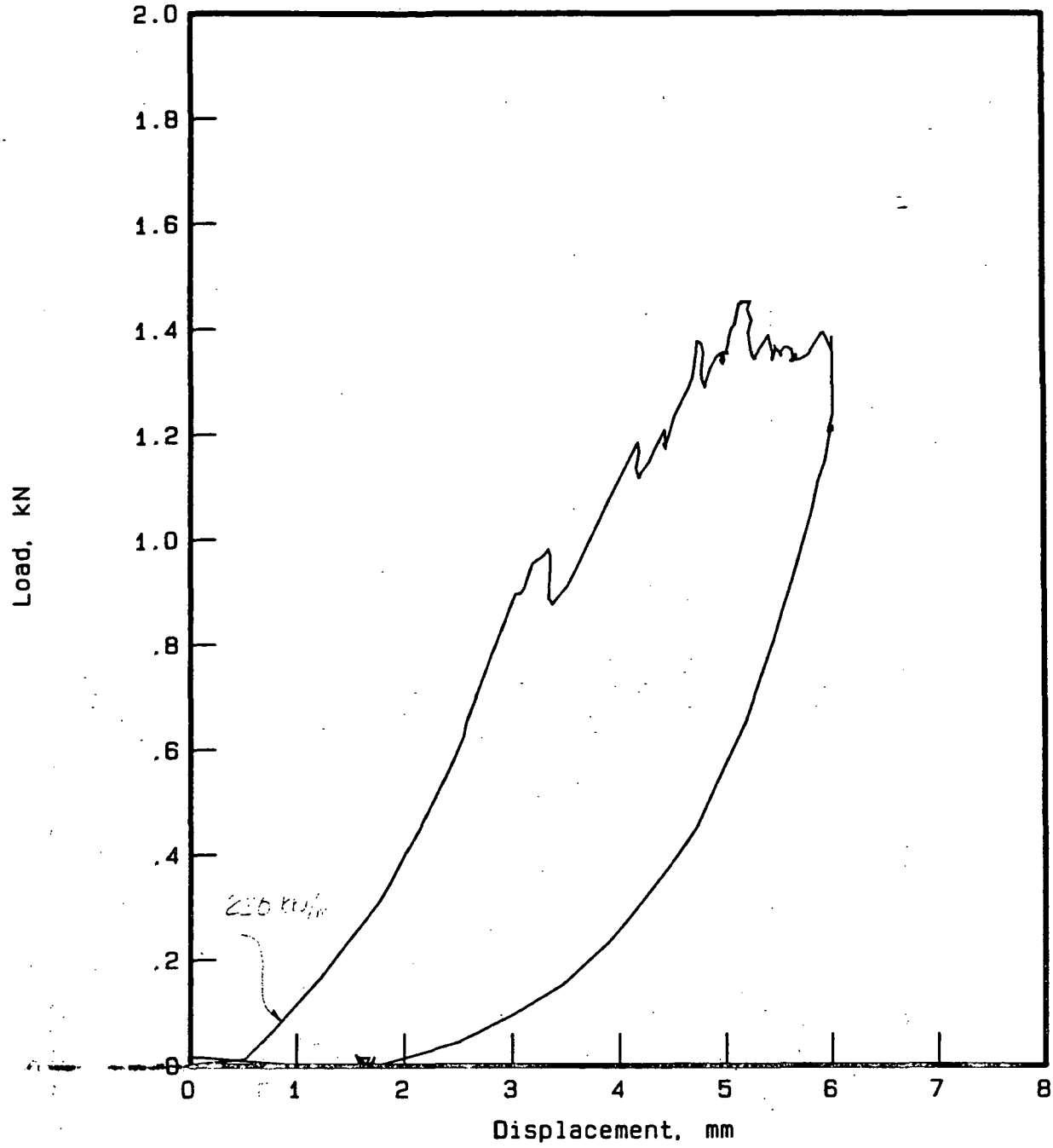

Fig. 2 - Load vs. Displacement Curve for tape laminate

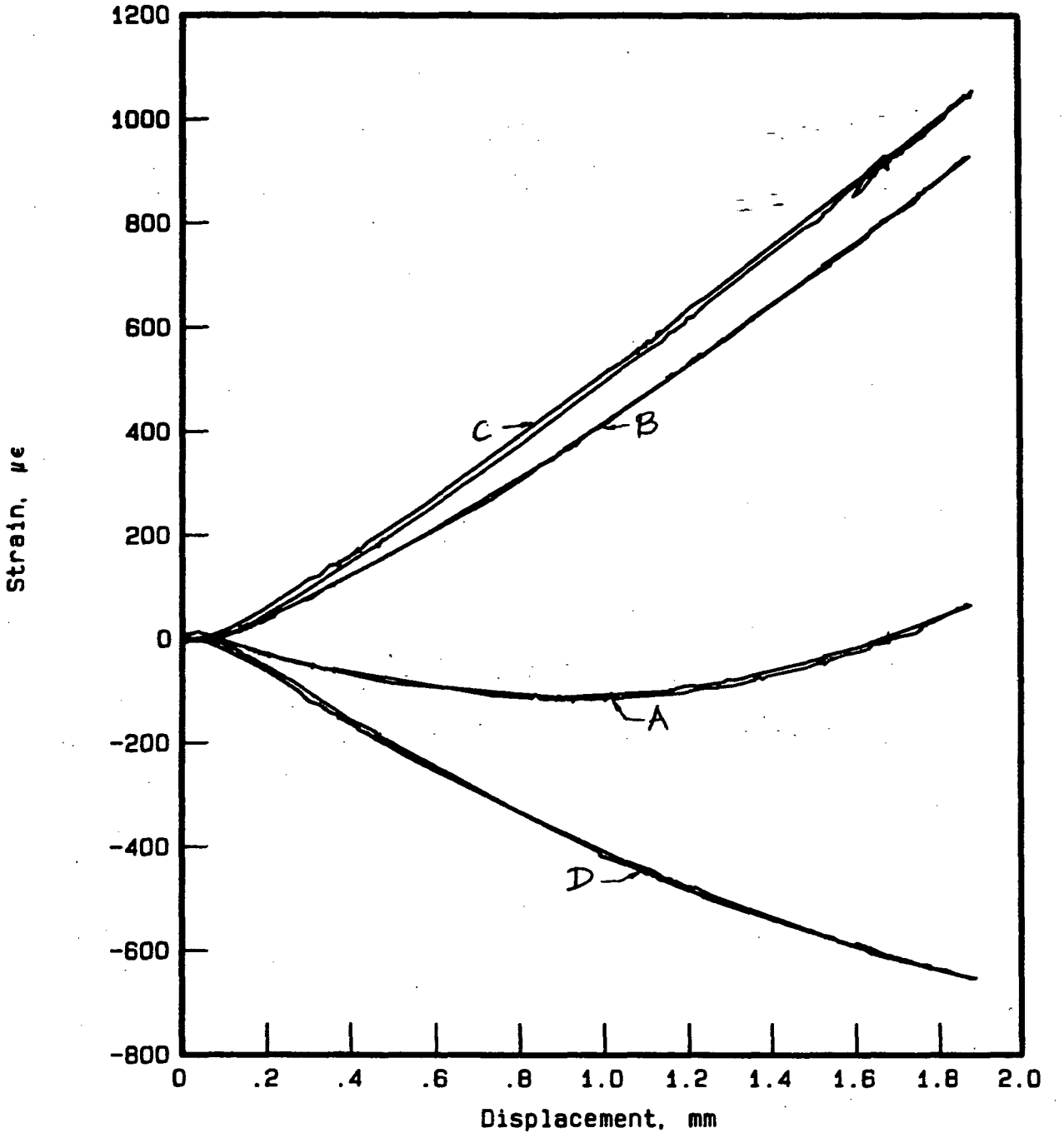

Static Indentation Test
Specimen A-5-02
Strains: A - top, r = 15.9 mm
B - bottom, r = 15.9 mm
C - top, r = 47.6 mm
D - bottom, r = 47.6 mm

Fig. 3a. - Strain vs. Displacement Curves for Static Indentation Tests

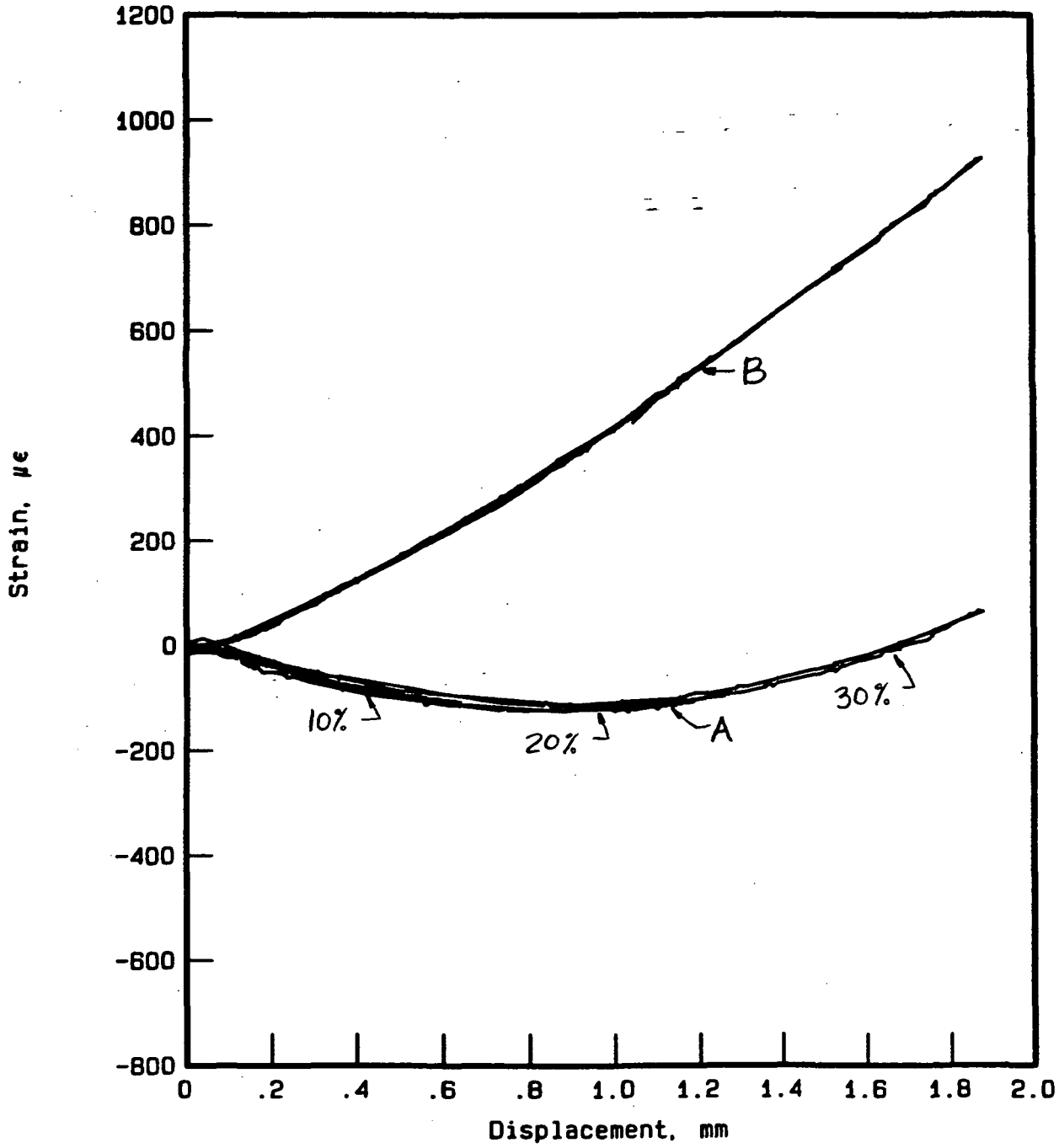

Static Indentation Test
Specimen A-5-02
Strains A & B : Top & Bottom Surface, r = 15.9 mm
10%, 20%, 30% of maximum displacement

Fig. 3b. - Strain vs. Displacement Curves for Static Indentation Tests

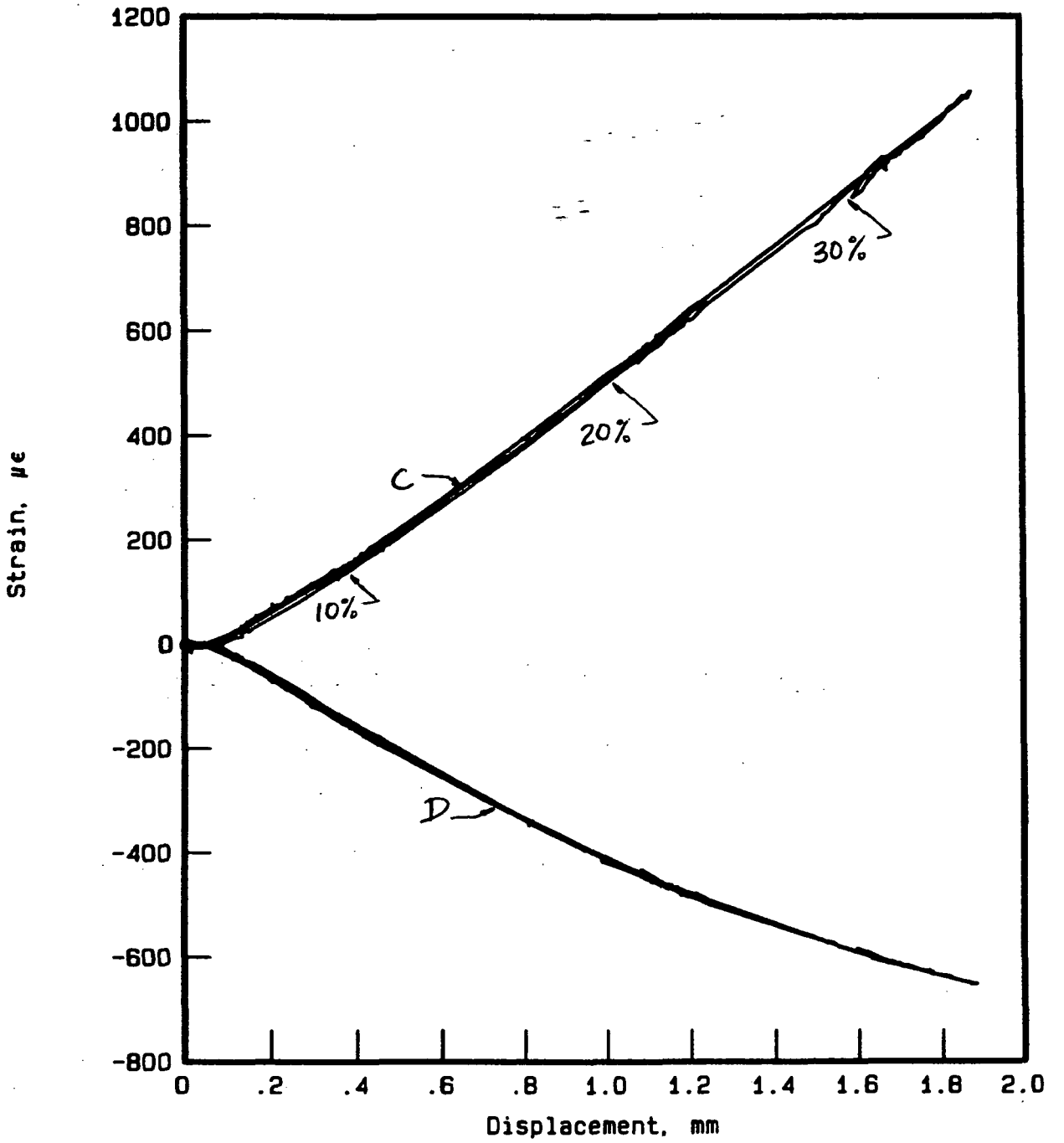

Static Indentation Test
Specimen A-5-02
Strains C & D : Top & Bottom, r = 47.6 mm
10%, 20%, 30% of maximum displacement

Fig. 3c. - Strain vs. Displacement Curves for Static Indentation Tests

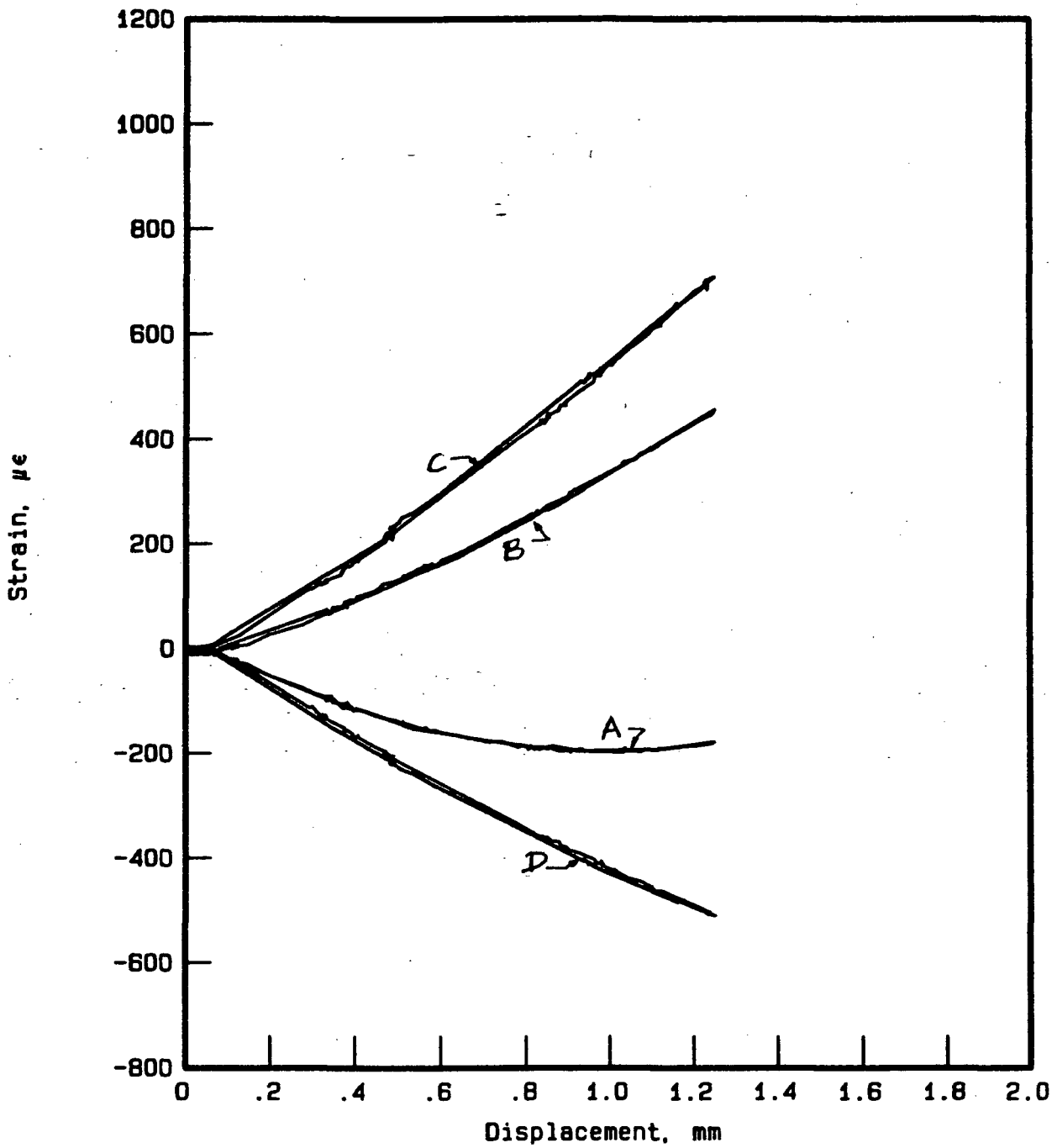

Static Indentation Test
Specimen A-5-3
Strains A, B, C, D - same as Specimen A-5-02

Fig. 4 - Strain vs. Displacement Curves for Static Indentation Tests

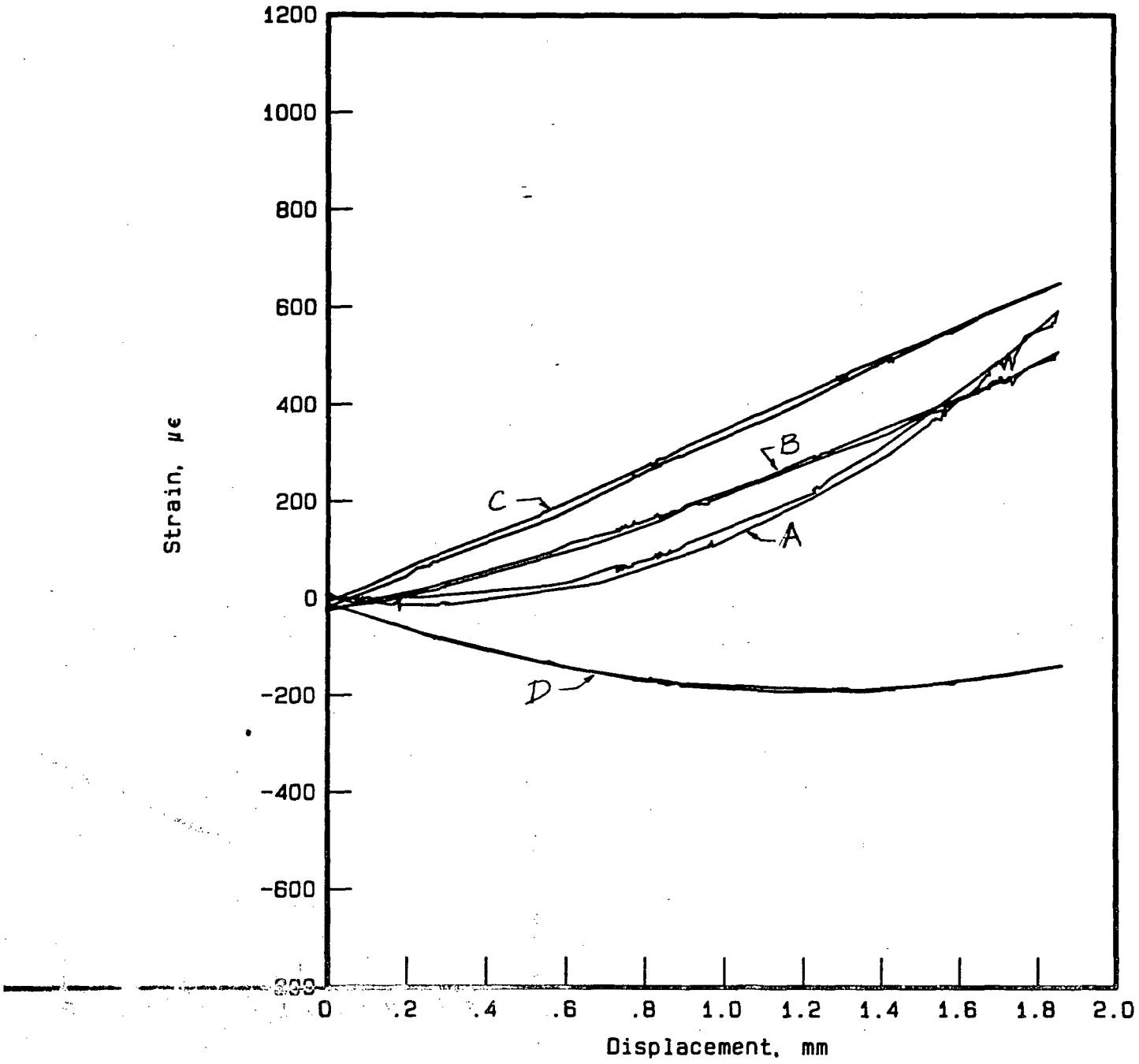

Static Indentation Test
Specimen B-5-3
Strains A, B, C, D
same as A-5-02

Fig. 5 - Strain vs. Displacement Curves for Static Indentation Tests

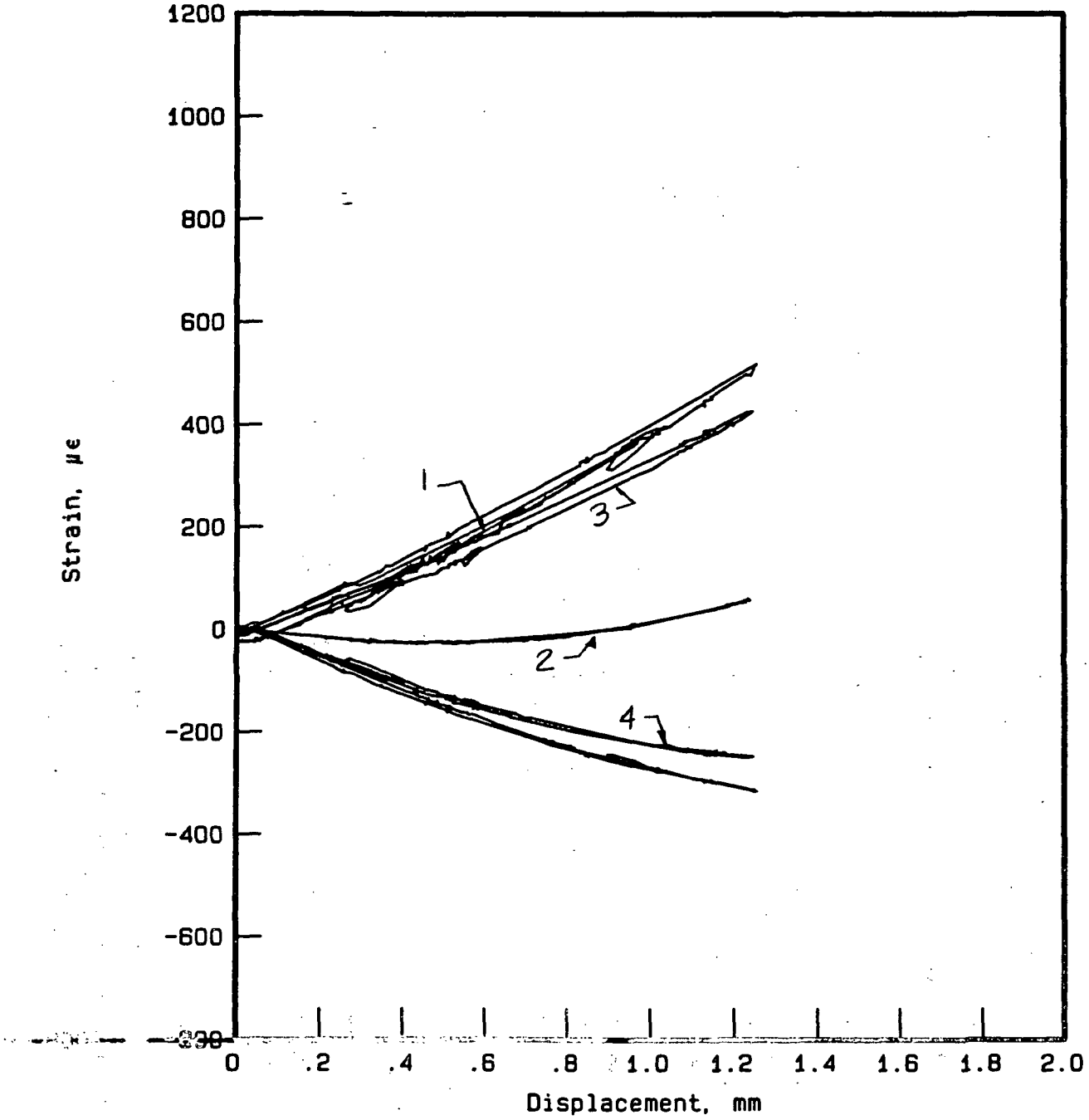

Static Indentation Test
Specimen B-5-4
Strain: A & 2 - Top & Bottom r = 23.5 mm
3 & 4 - Top & Bottom, r = 47.6 mm

Fig. 6 - Strain vs. Displacement Curves for Static Indentation Tests

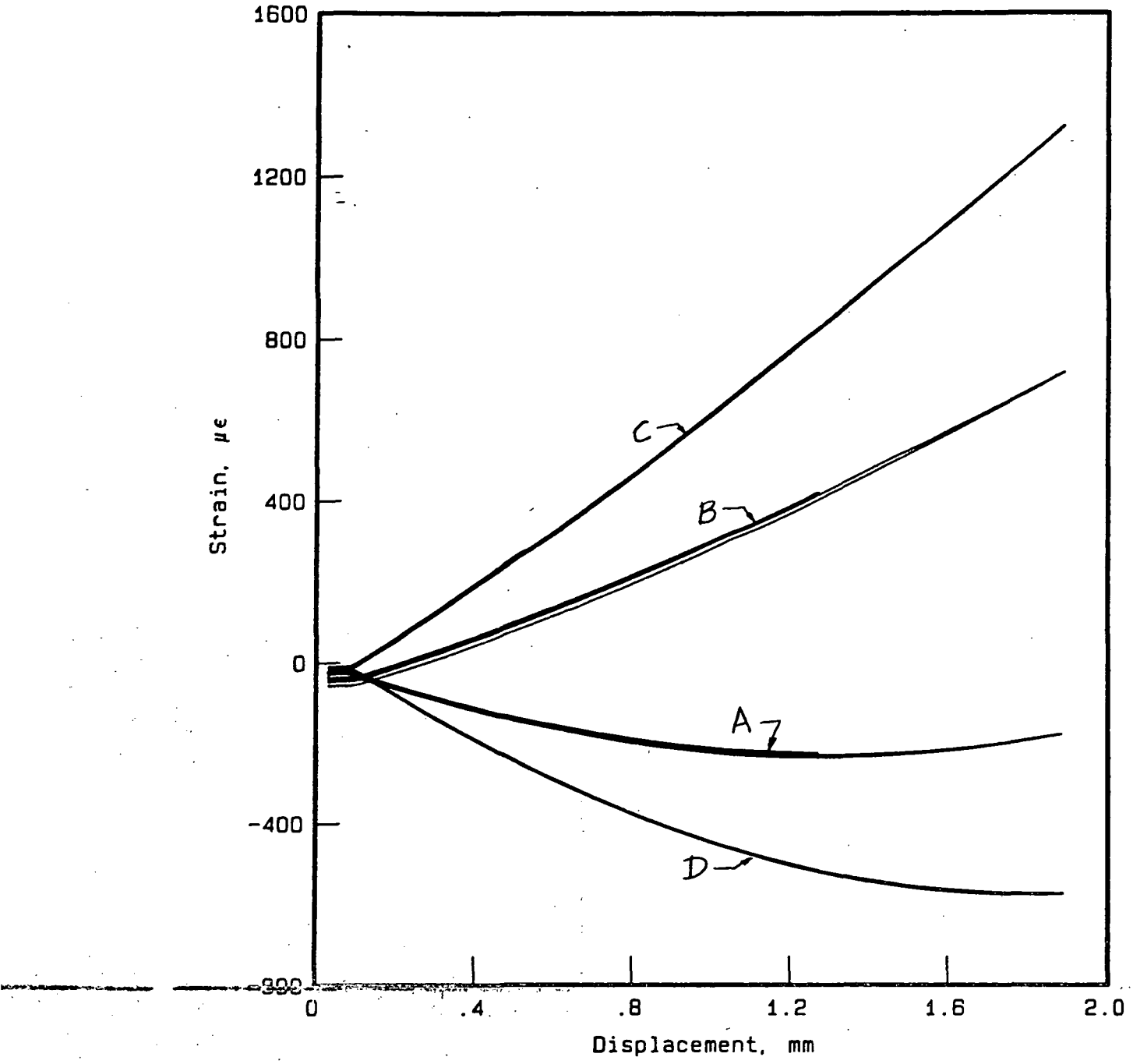

Static Indentation Test
Specimen A-S-B1 - 5"x 1" Beam
Strain A & B - Top & Bottom r= 23.5 mm
C & D - Top & Bottom r= 47.6 mm

Fig. 7 - Strain vs. Displacement Curves for Static Indentation Tests

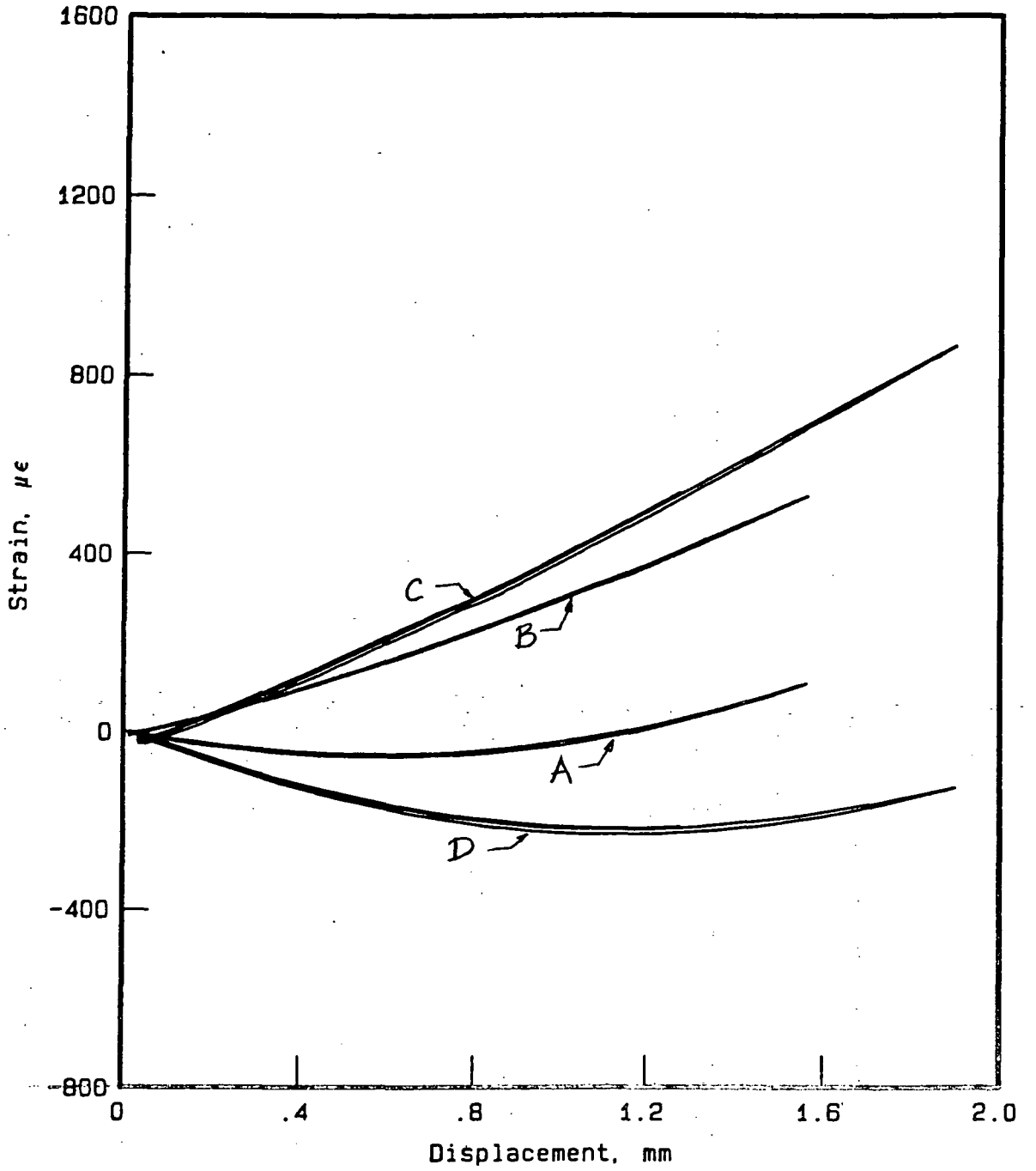

Static Indentation Test
Specimen B-S-B1 - 5"x 1" Beam
Strain : A & B Top & Bottom r= 23.5 mm
C & D Top & Bottom r= 47.6 mm

Fig. 8 - Strain vs. Displacement Curves

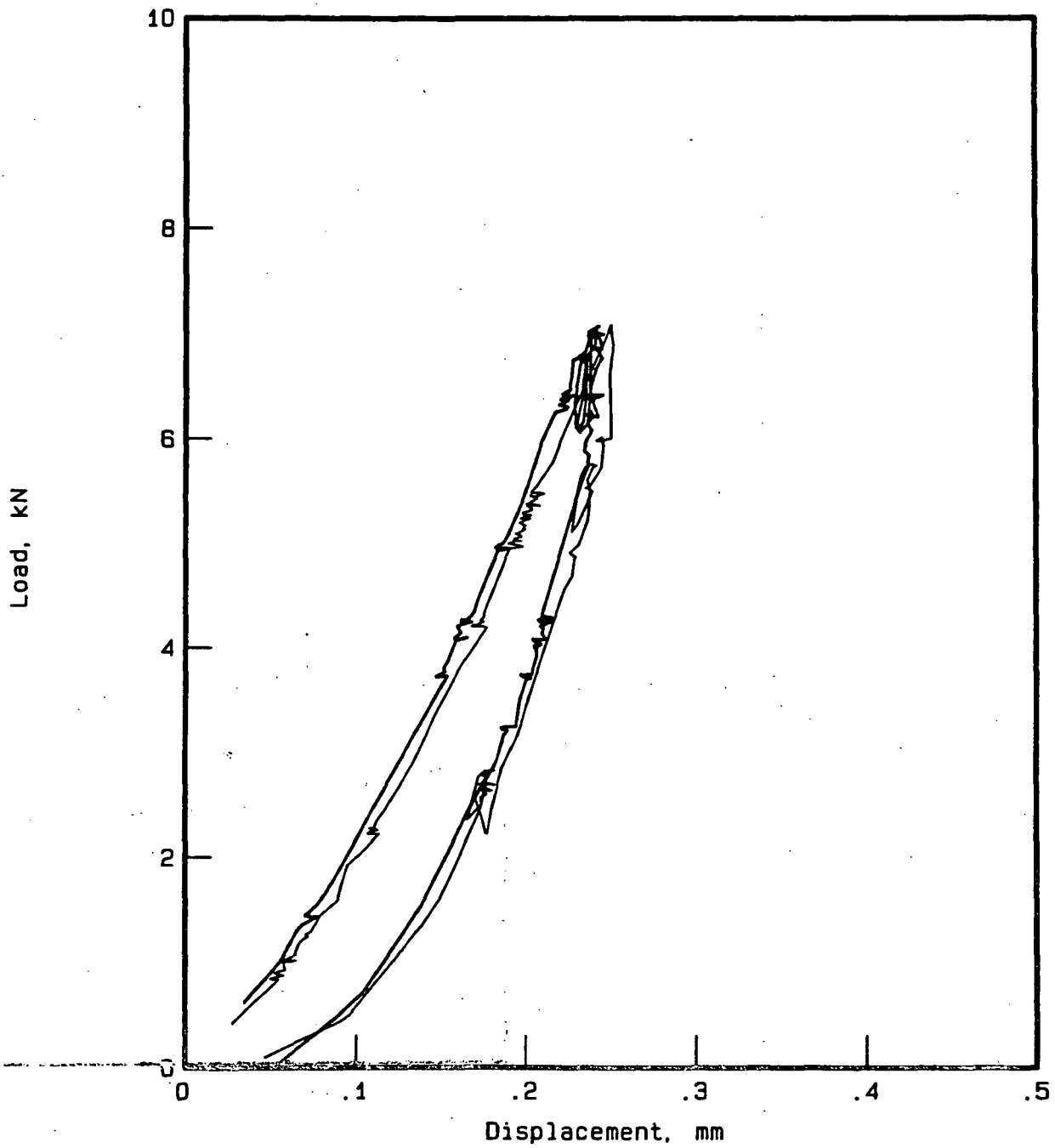

Indentation Test

Fig. 9 - Load vs. Displacement Curve for fully backed woven fabric laminate

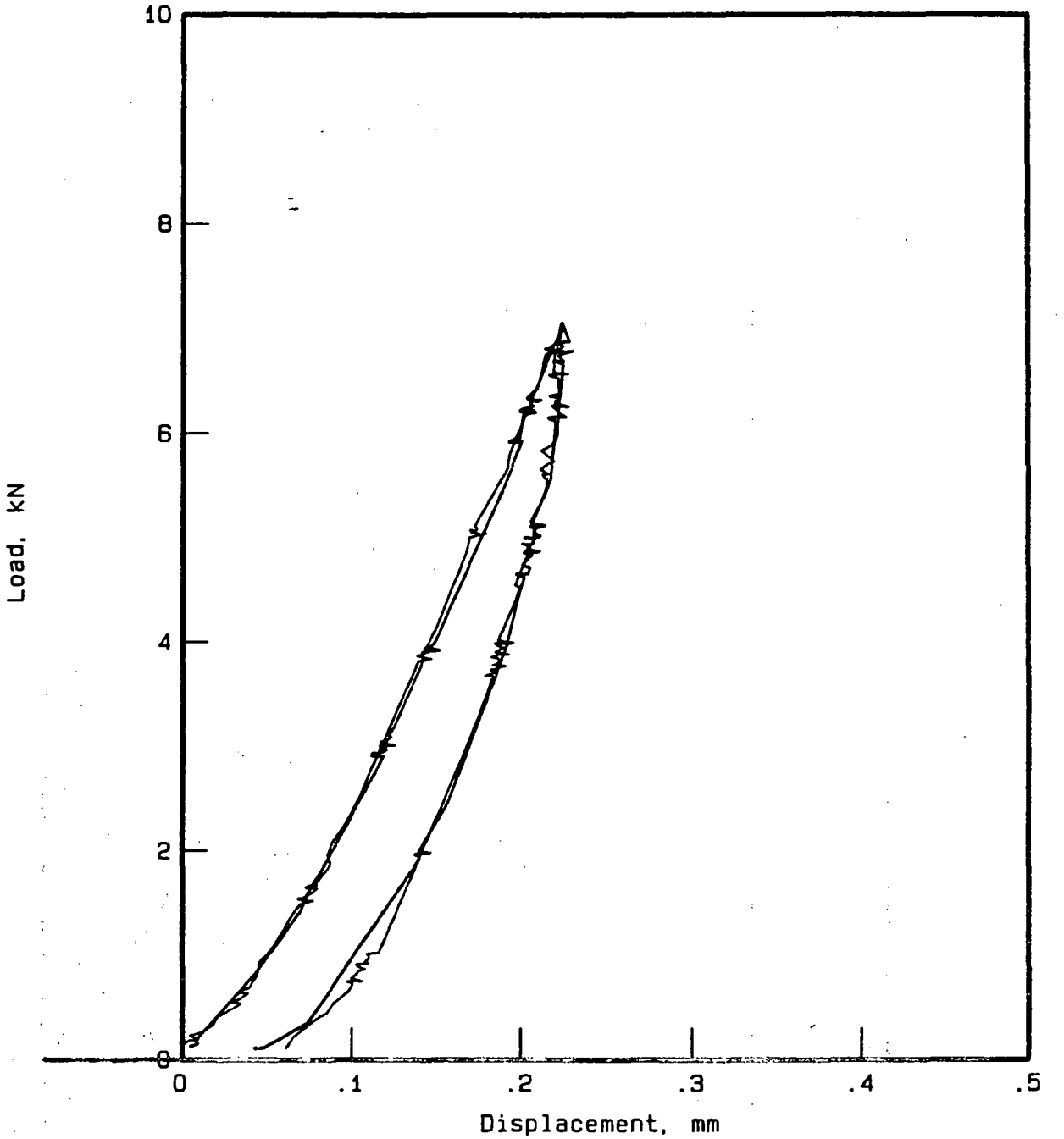

Indentation Test

Fig. 10 - Load vs. Displacement Curve for fully backed tape laminate

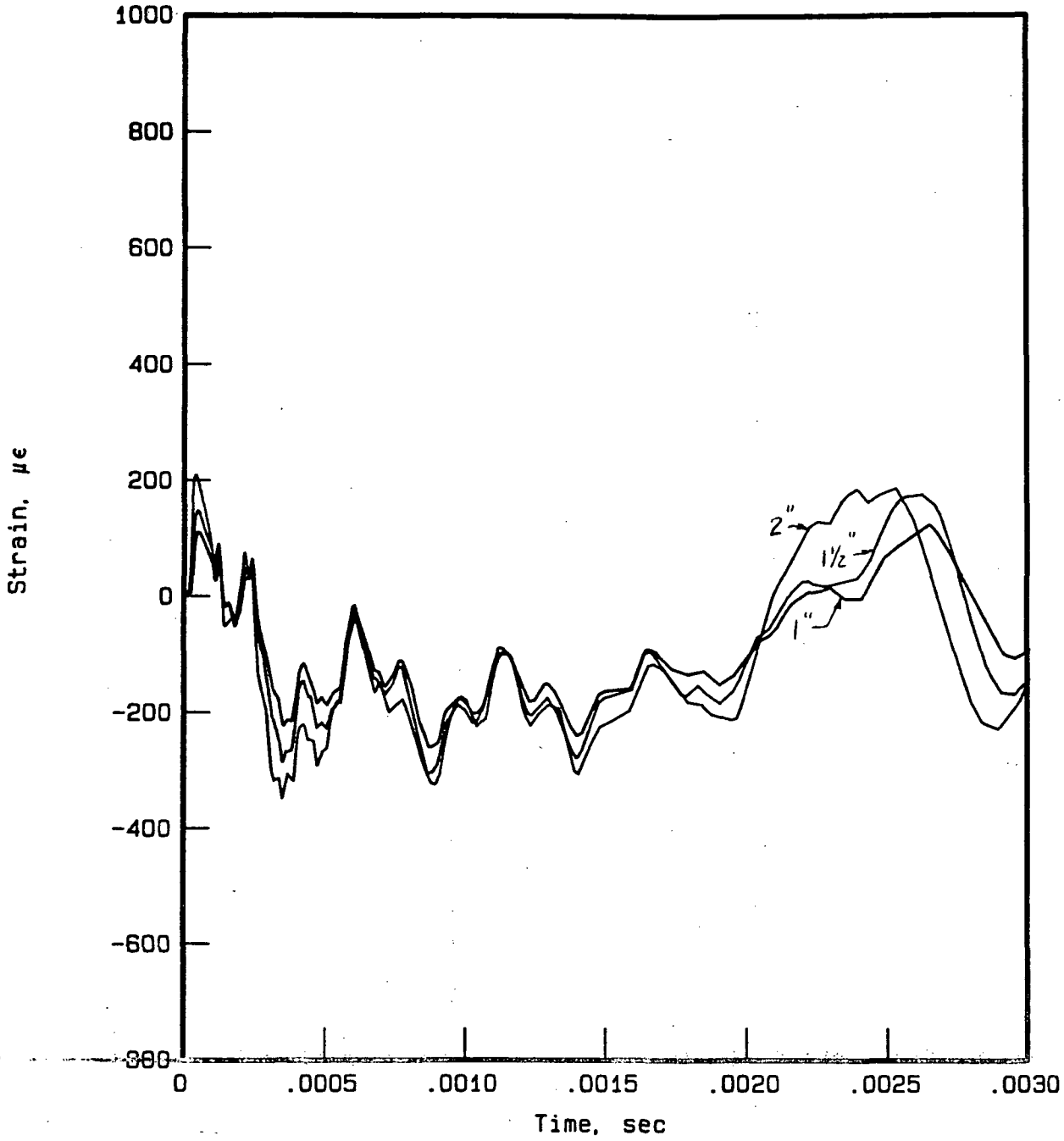

Low-velocity Impact Test
Specimen A-5-3
Strain A : Top Surface at r = 15.9mm

Fig. 11-A

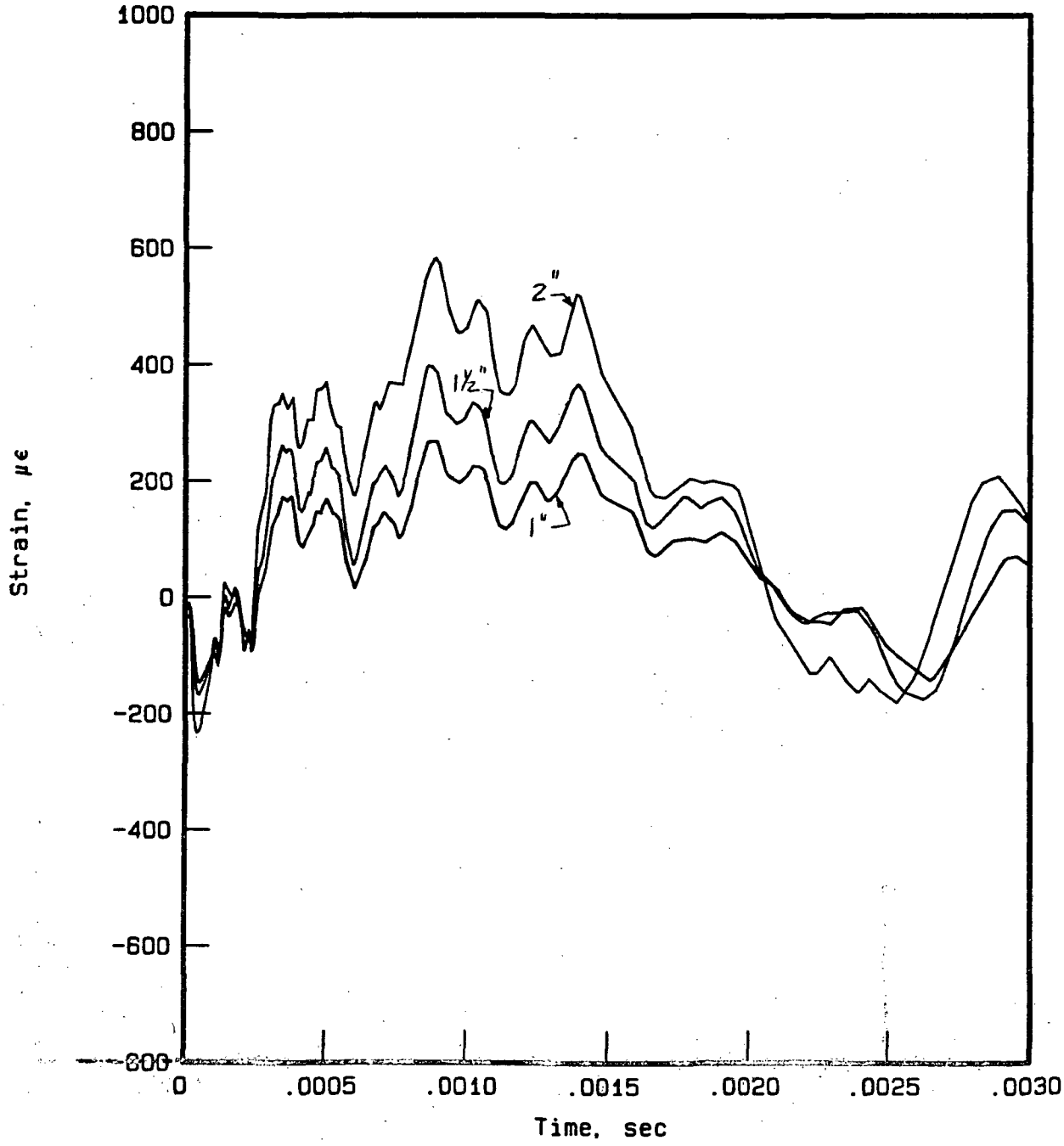

Low-velocity Impact Test
Specimen A-5-3
Strain B : Bottom Surface at r = 15.9 mm

Fig. 11-B

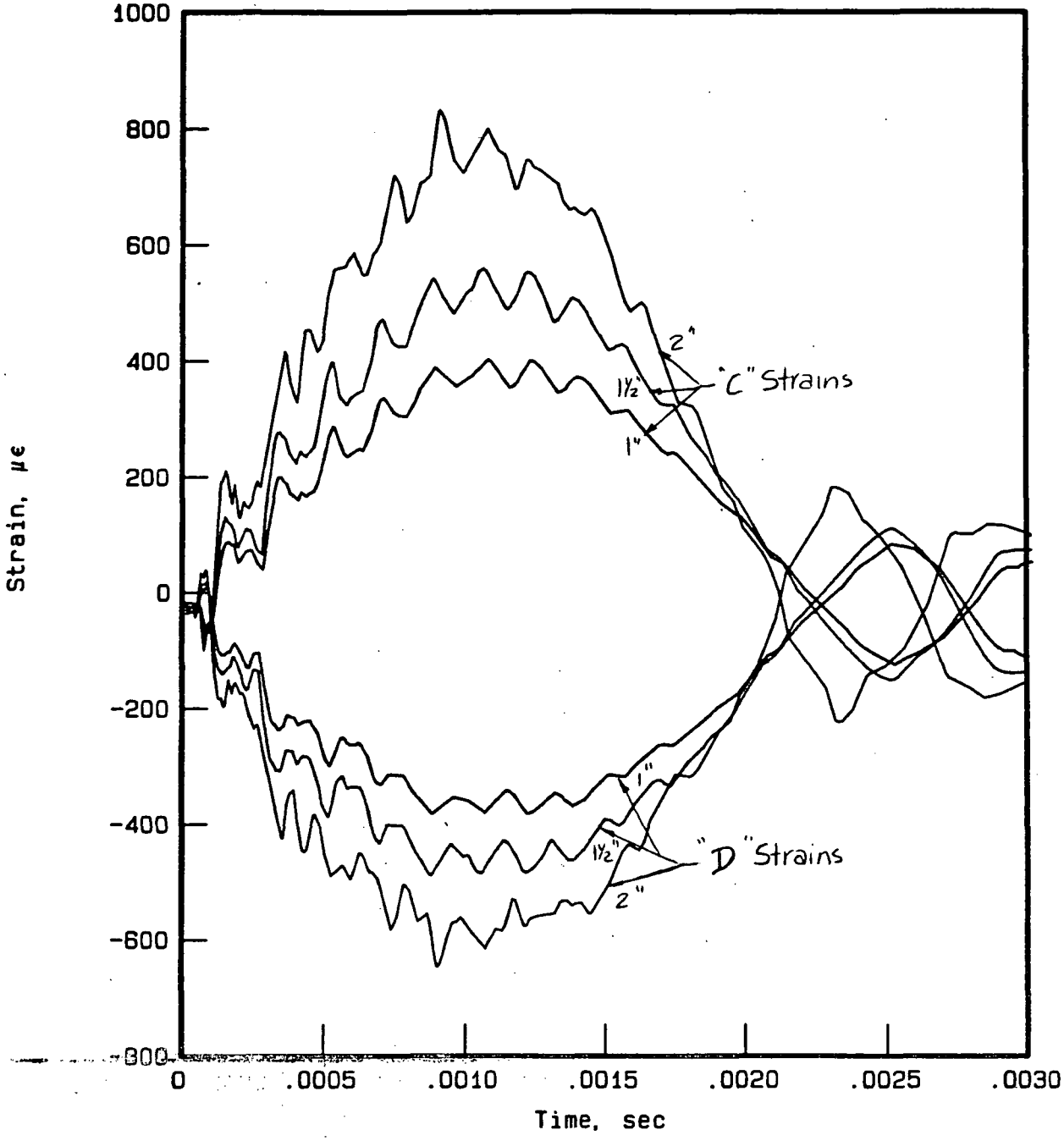

Low-velocity Impact Test
Specimen A-5-3
Strains C & D : Top & Bottom Surfaces at r = 47.6 mm

Fig. 11-C,D

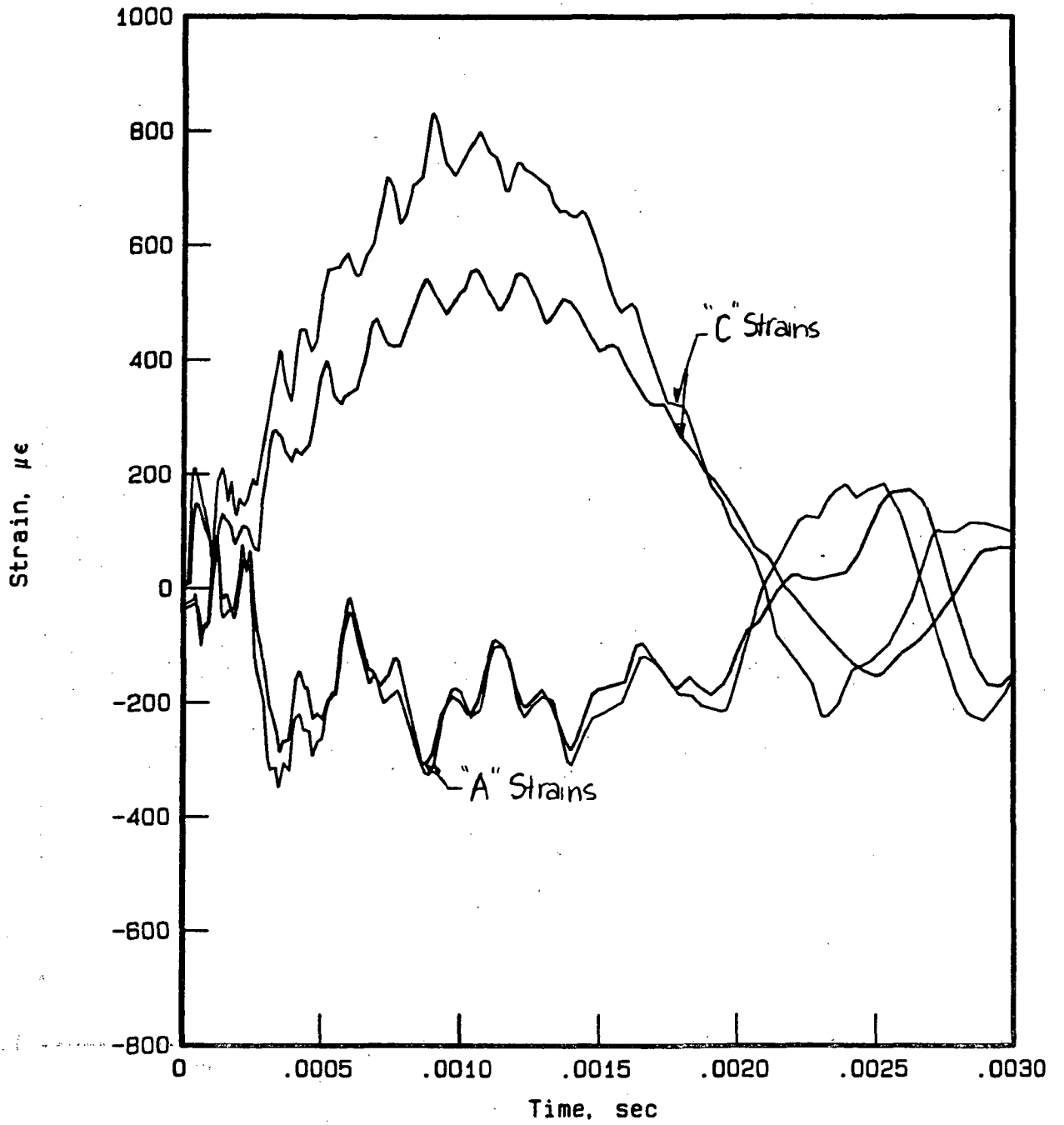

Low-velocity Impact Test
Specimen A-5-3
Strains A & C Top Surface at r = 15.9 mm & r = 47.6 mm

Fig. 11 - A,C

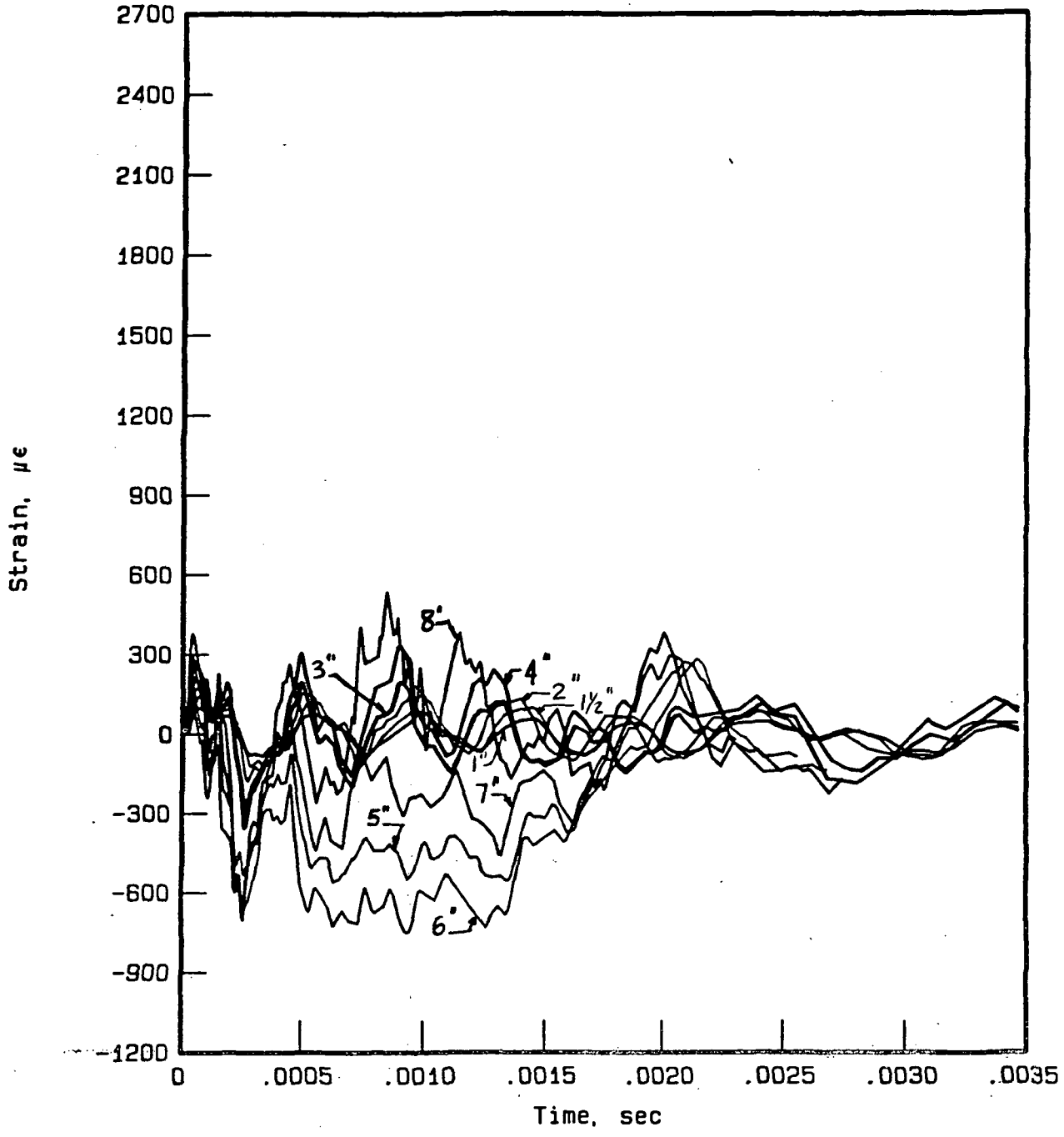

Low-Velocity Impact Test

Specimen A-D-5

Strain A : Top Surface at r = 23.5 mm

0° direction

Fig. 12-A

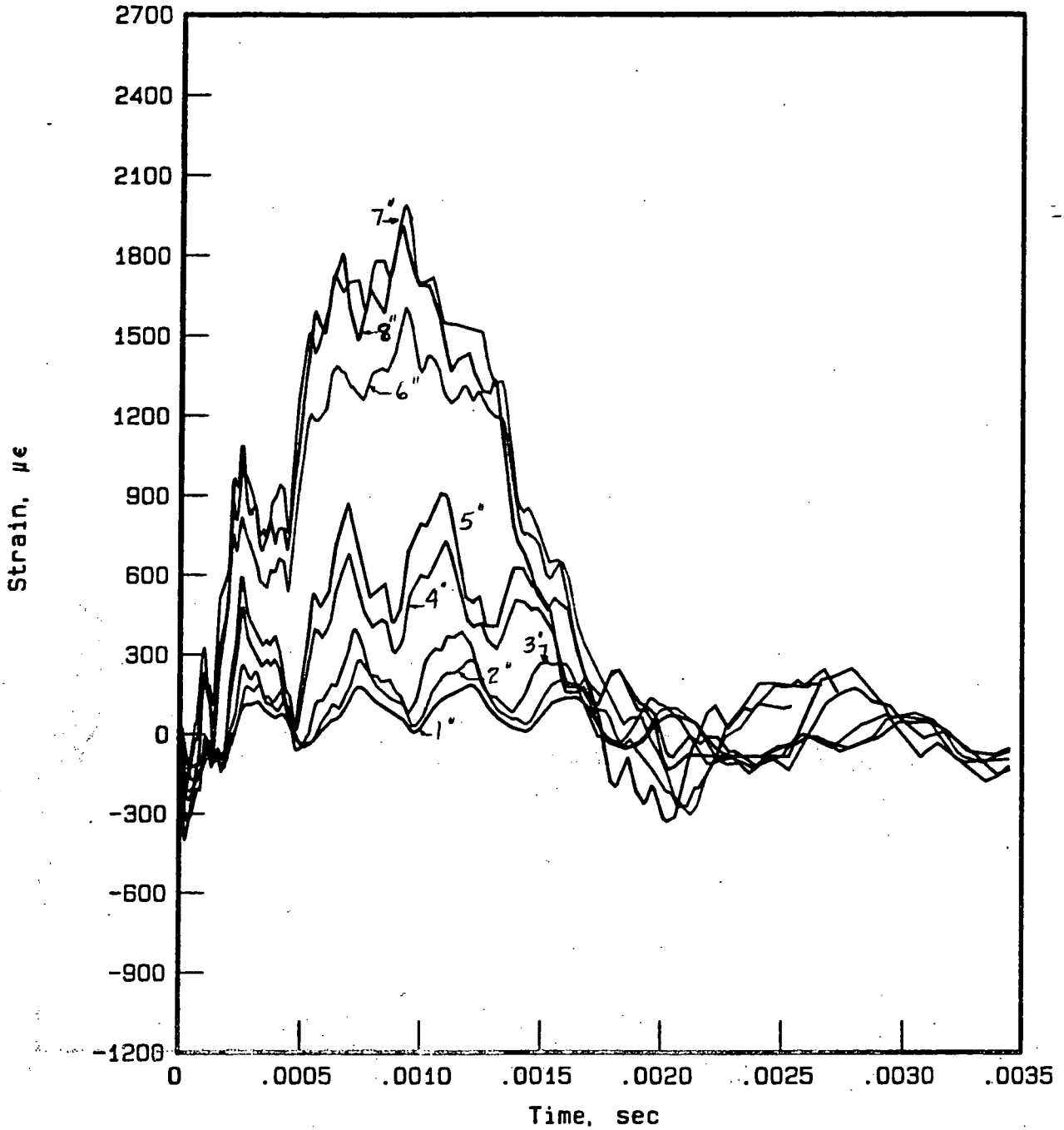

Low-Velocity Impact Test
Specimen A-D-5
Strain B : Bottom Surface at r = 23.5 mm

Fig. 12-B

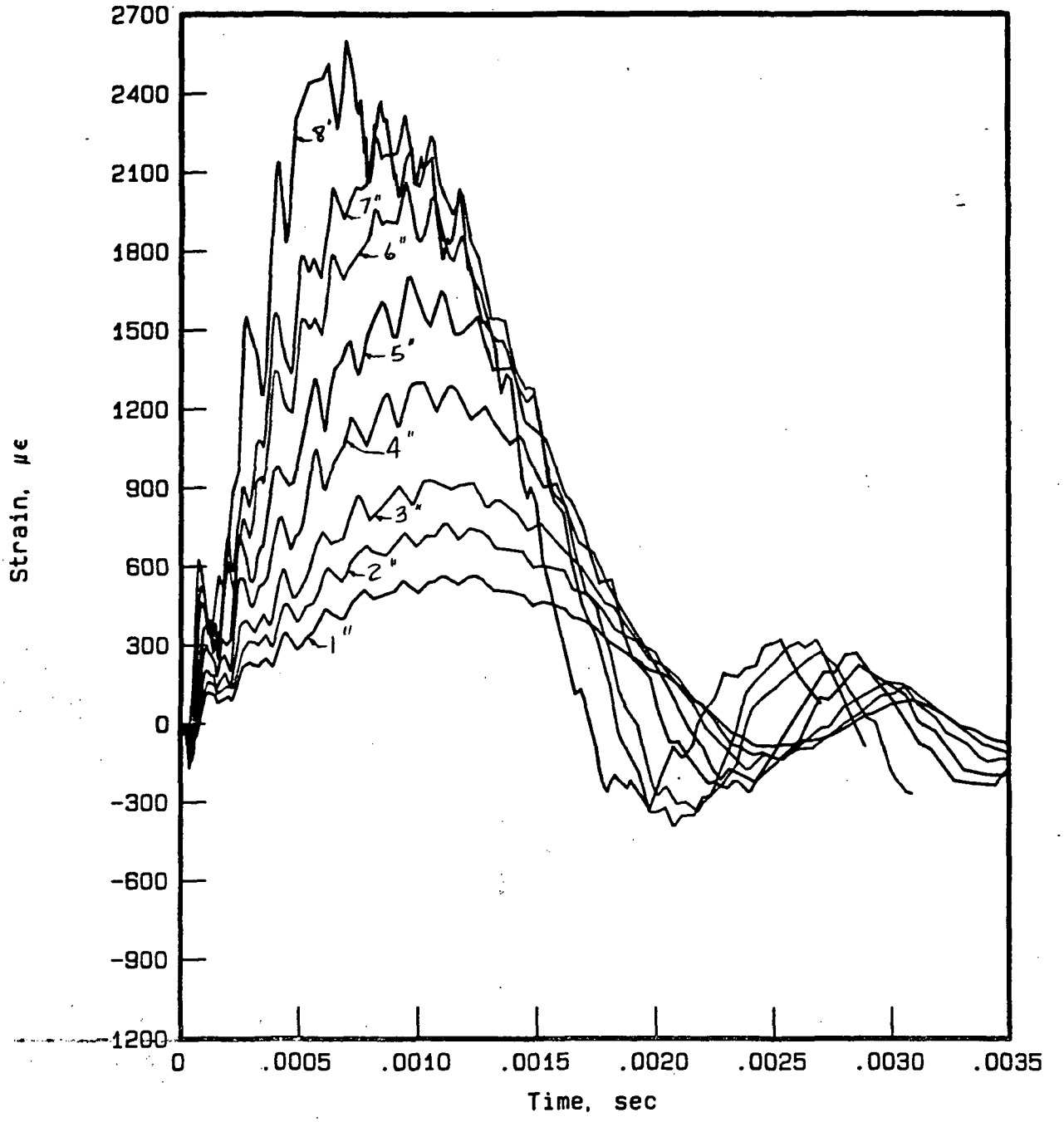

Low-Velocity Impact Test
Specimen A-D-5
Strain C : Top Surface at r = 47.6 mm

Fig. 12-C

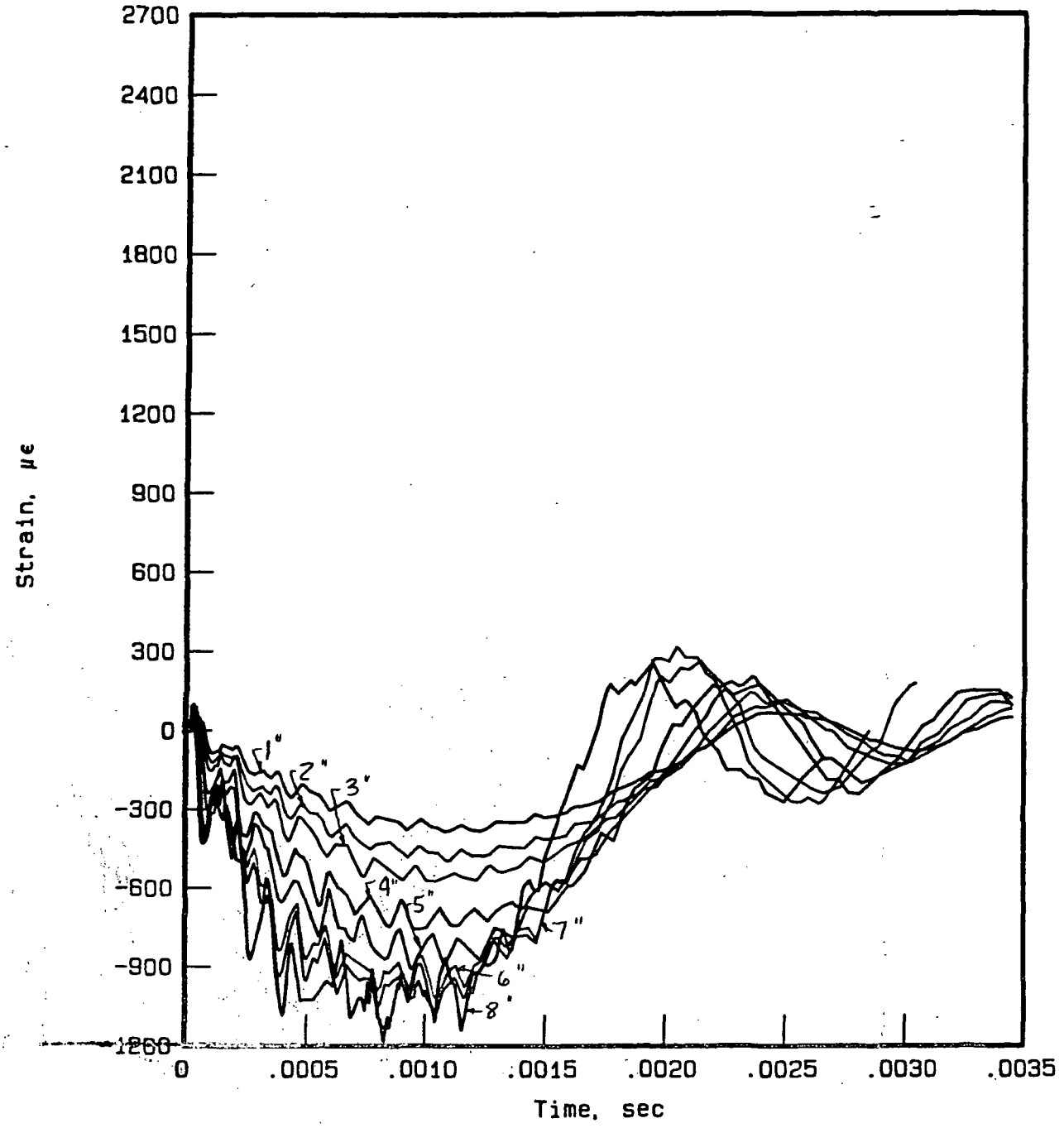

Low-Velocity Impact Test
Specimen A-D-5
Strain D : Bottom Surface at r = 47.6 mm

Fig. 12-D

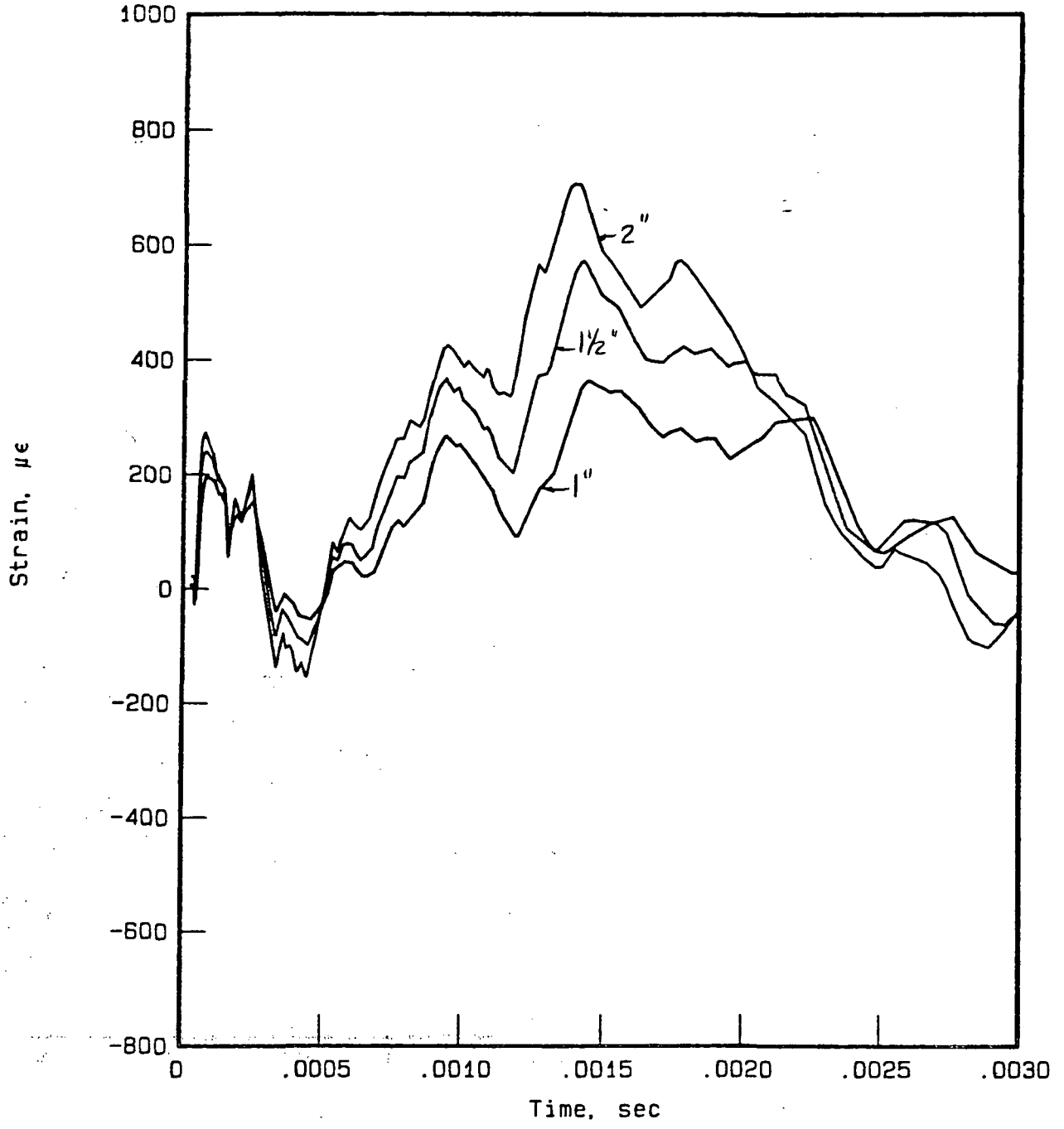

Low-velocity Impact Test
Specimen B-5-4
Strain A : Top Surface, r = 23.5 mm

Fig. 13-A

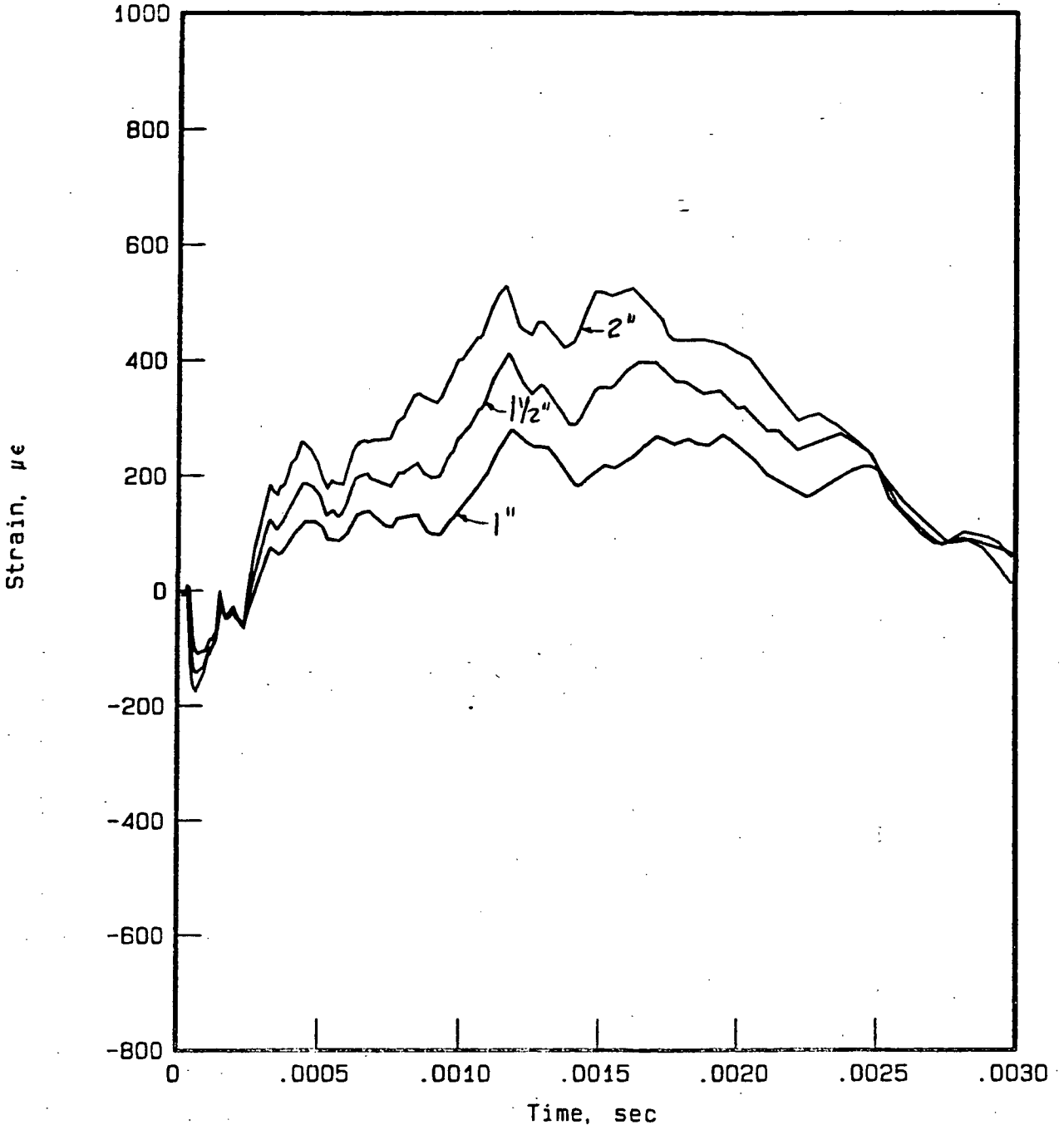

Low-velocity Impact Test
Specimen B-5-4
Strain B : Bottom Surface, r = 23.5mm

Fig. 13-B

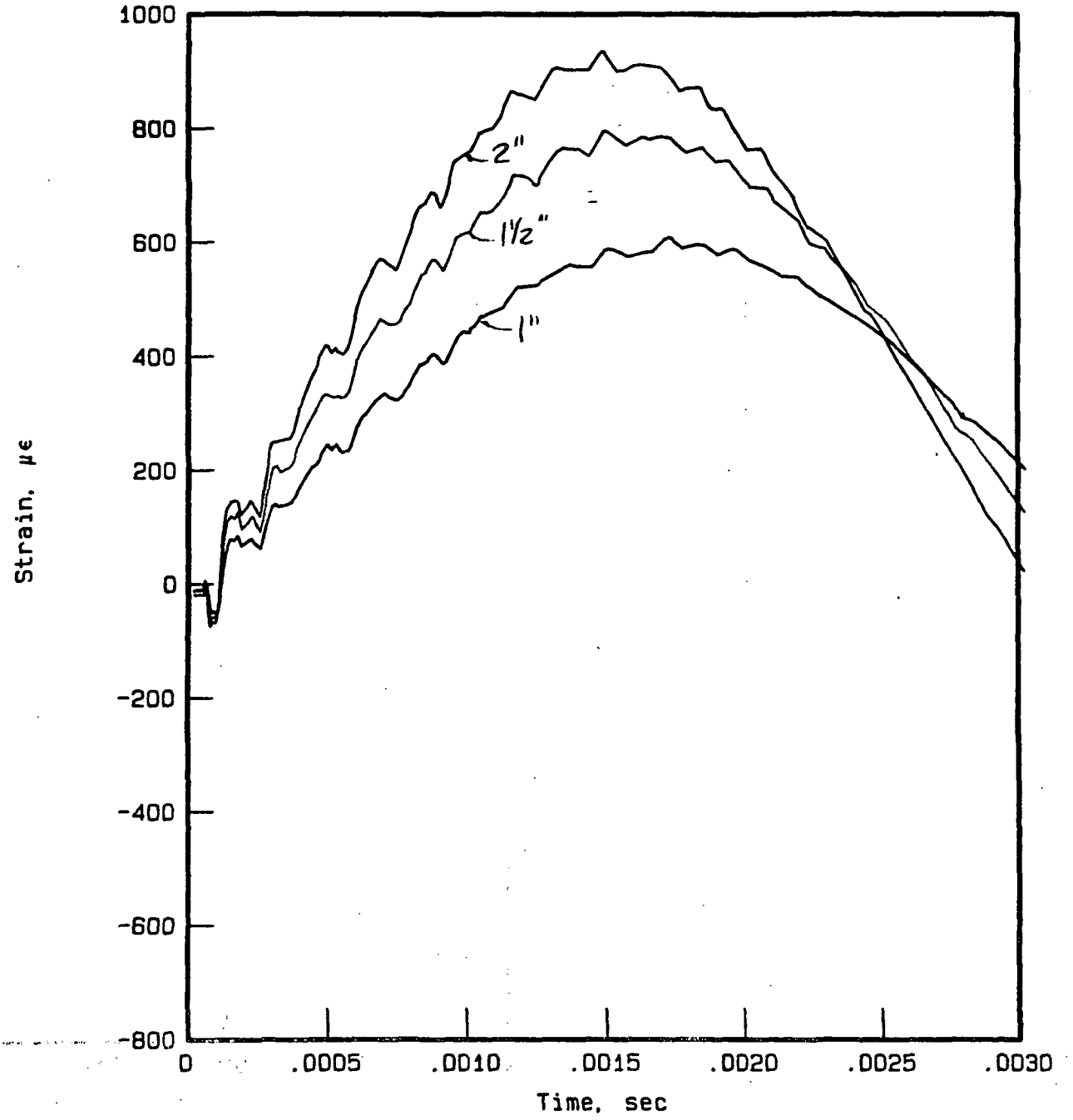

Low-velocity Impact Test
B-5-4
Strain C: Top Surface at r = 47.6mm

Fig. 13-C

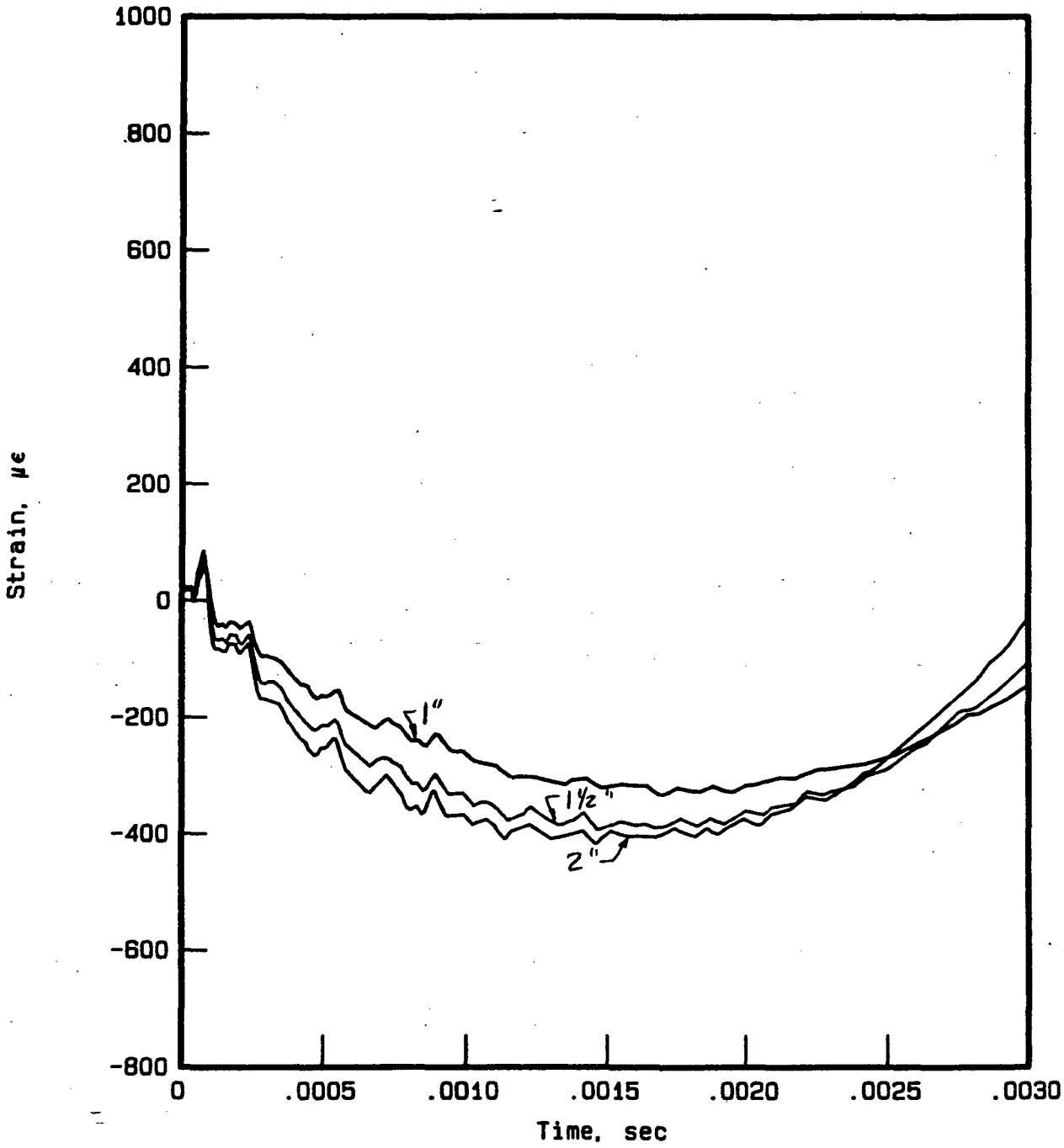

Low-velocity Impact Test
Specimen B-5-4
Strain D: Bottom Surface at r = 47.6 mm

Fig. 13-D

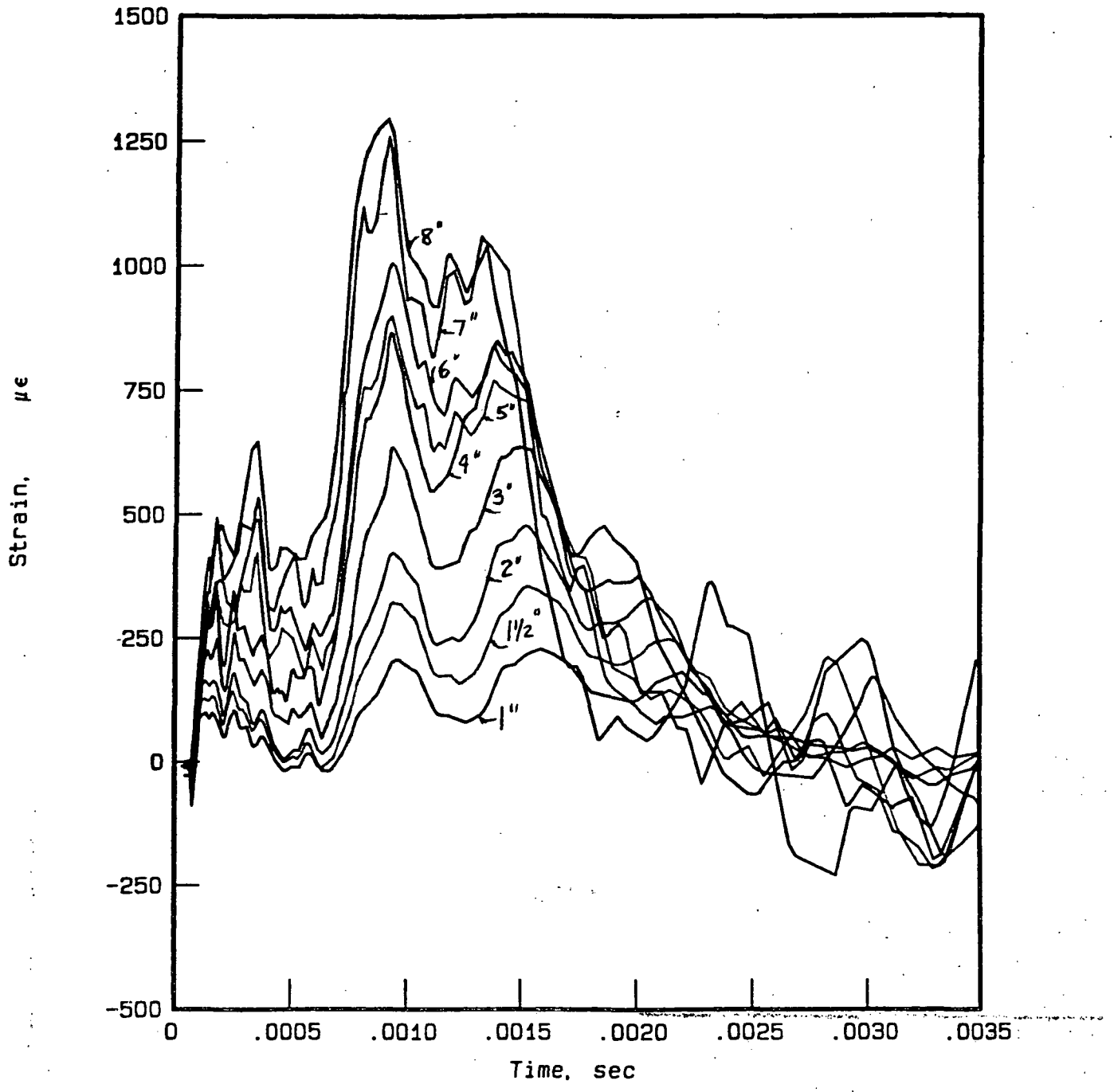

Low-Velocity Impact Test

Specimen B-D-5

Strain A : Top Surface at r = 23.5 mm

Fig. 14-A

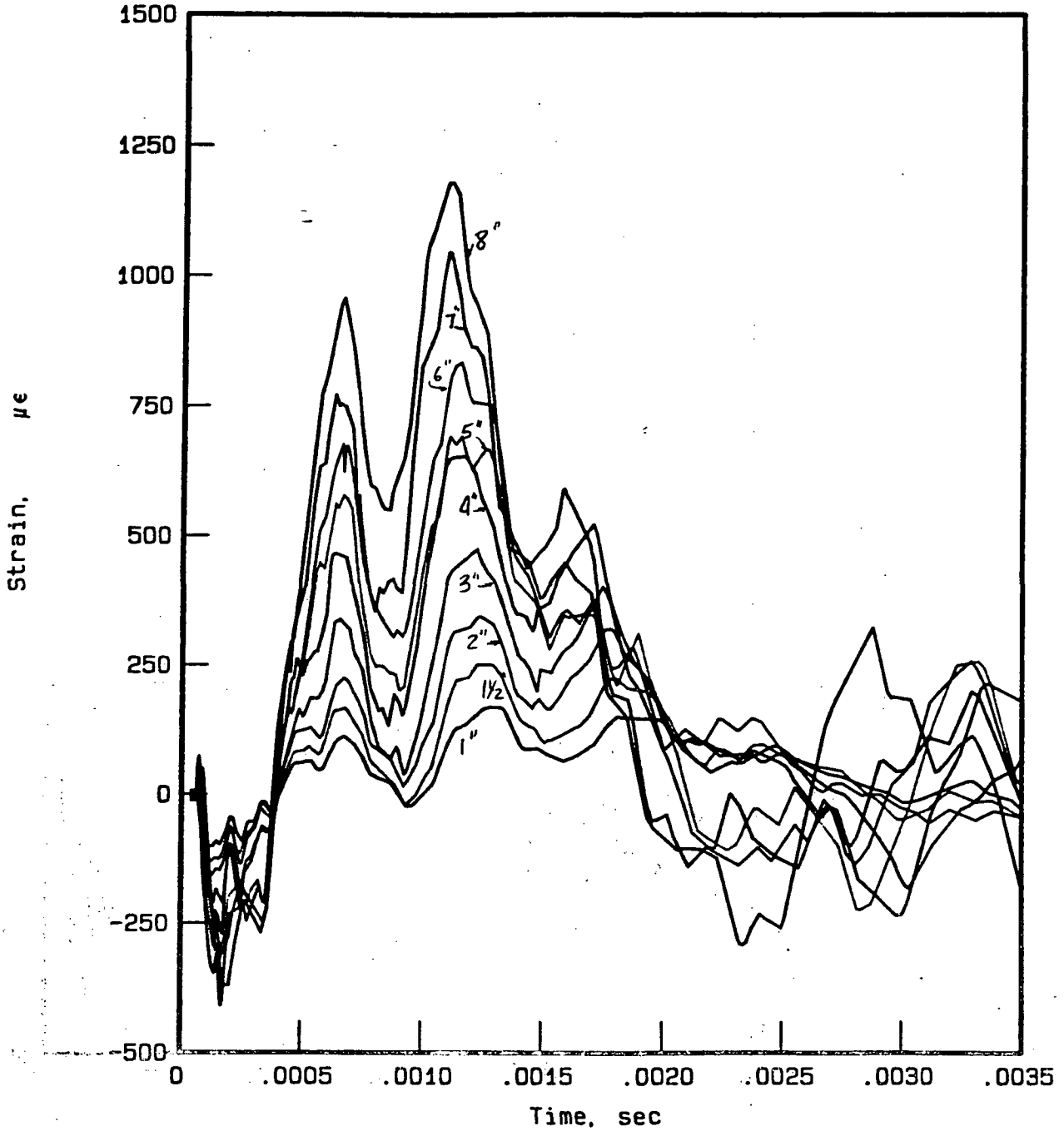

Low-Velocity Impact Test

Specimen B-D-5

Strain B: Bottom Surface at r = 23.5mm

Fig. 14-B

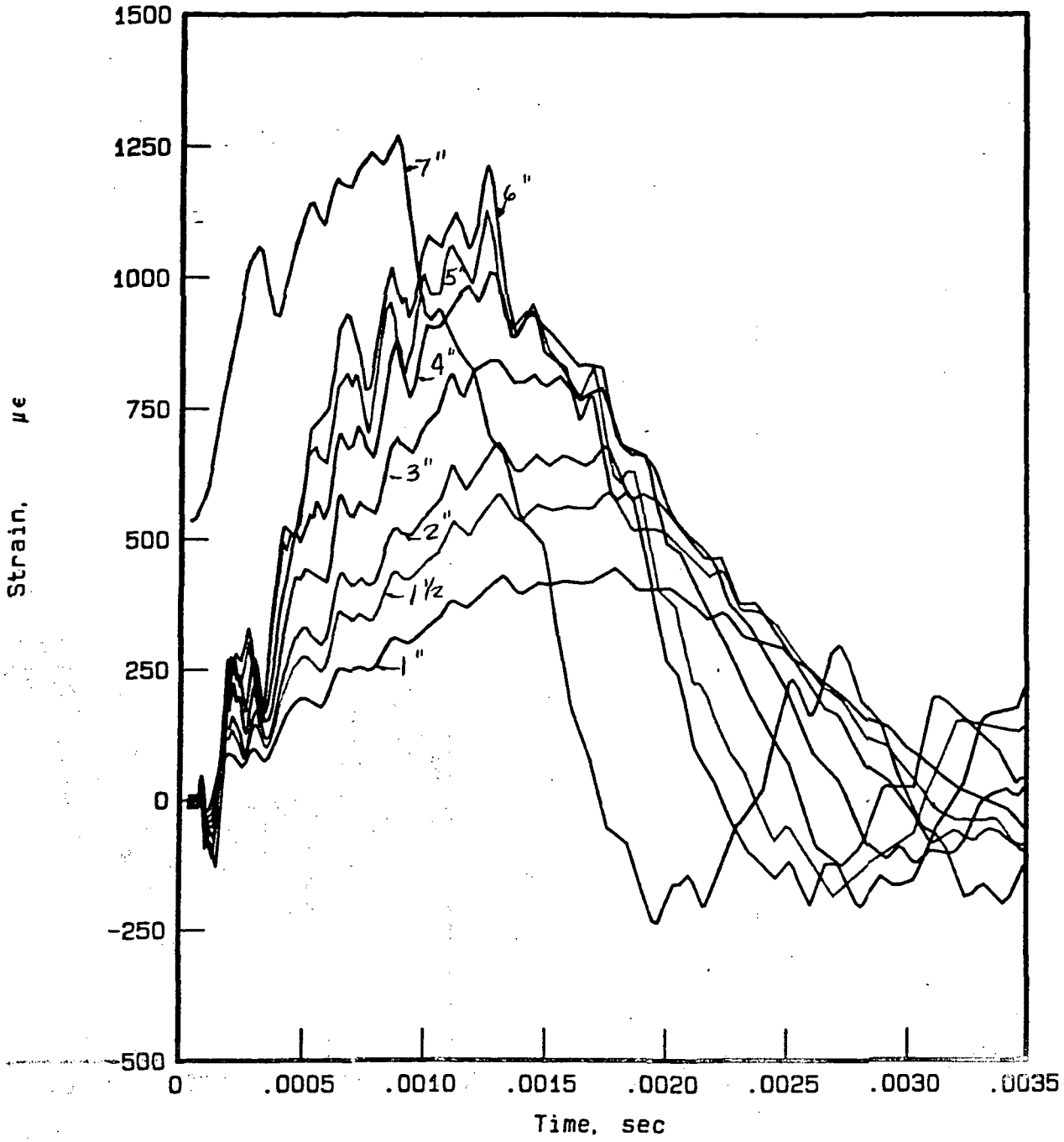

Low-Velocity Impact Test
Specimen B-D-5
Strain C : Top Surface at r = 47.6 mm

Fig. 14-C

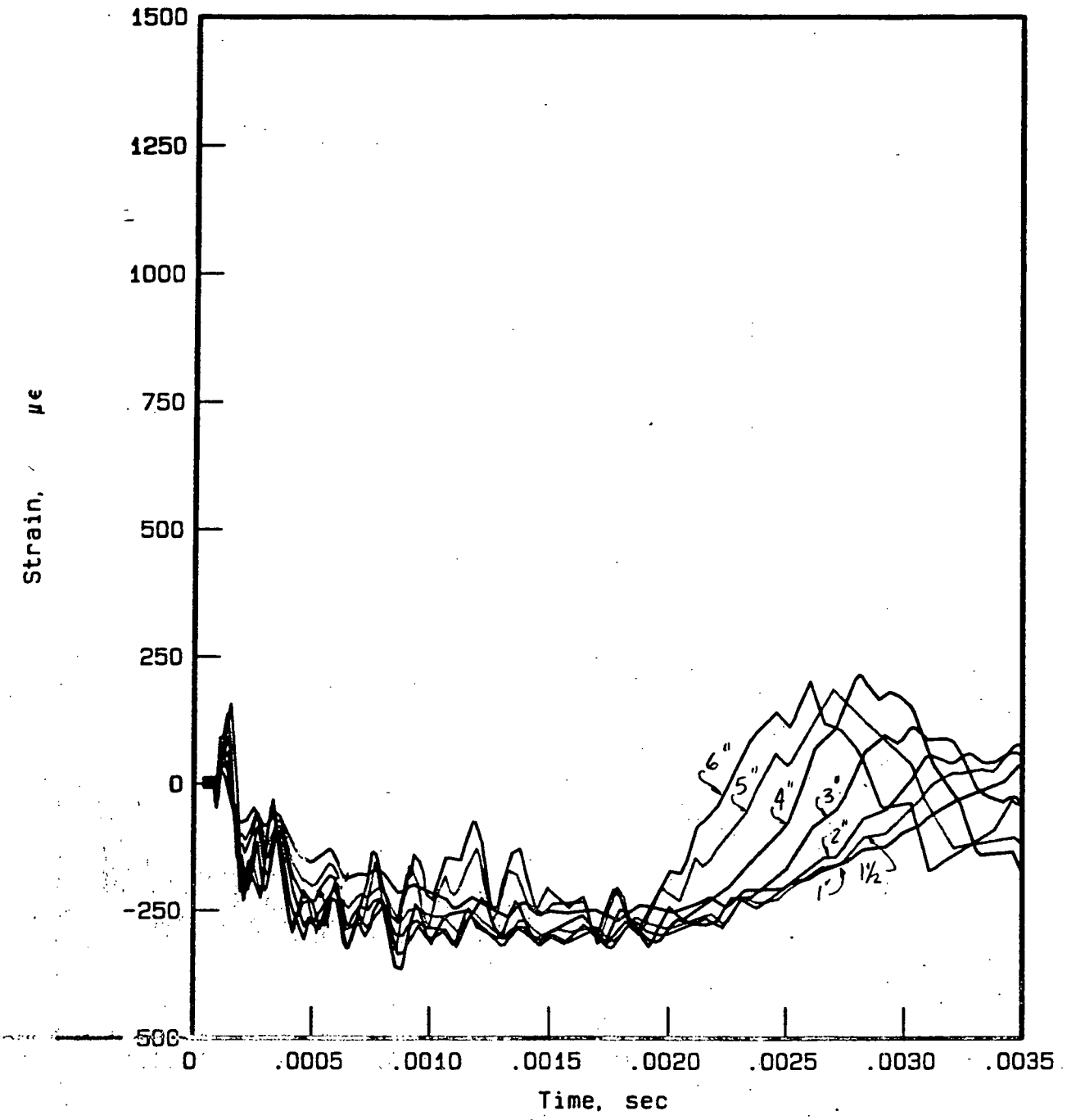

Low-Velocity Impact Test
Specimen B-D-5
Strain D: Bottom Surface, r = 47.6mm

Fig. 14-D

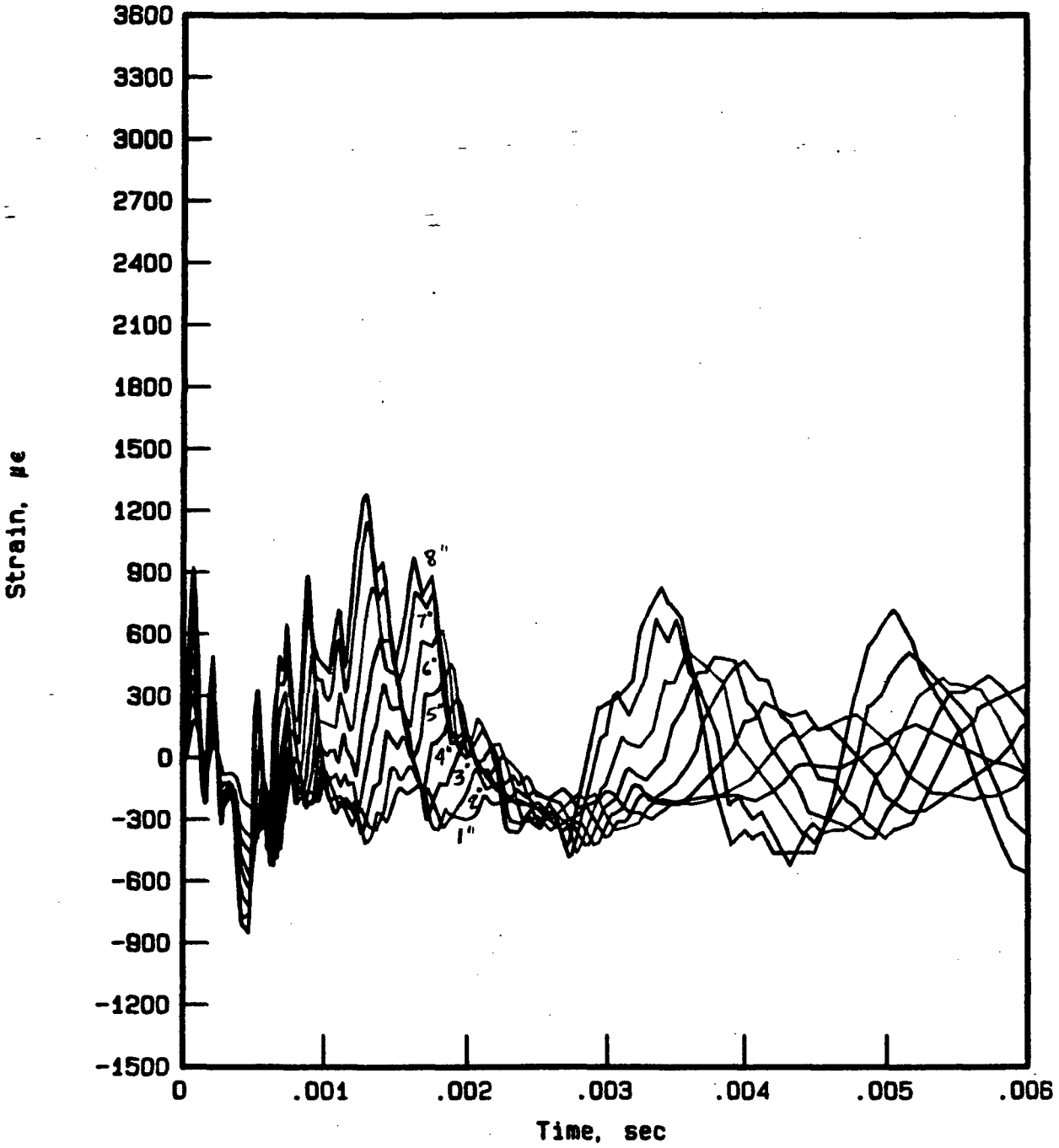

Low-Velocity Impact Test on 5" length Beam
Specimen A-D-B
Strain A

Fig. 15-A

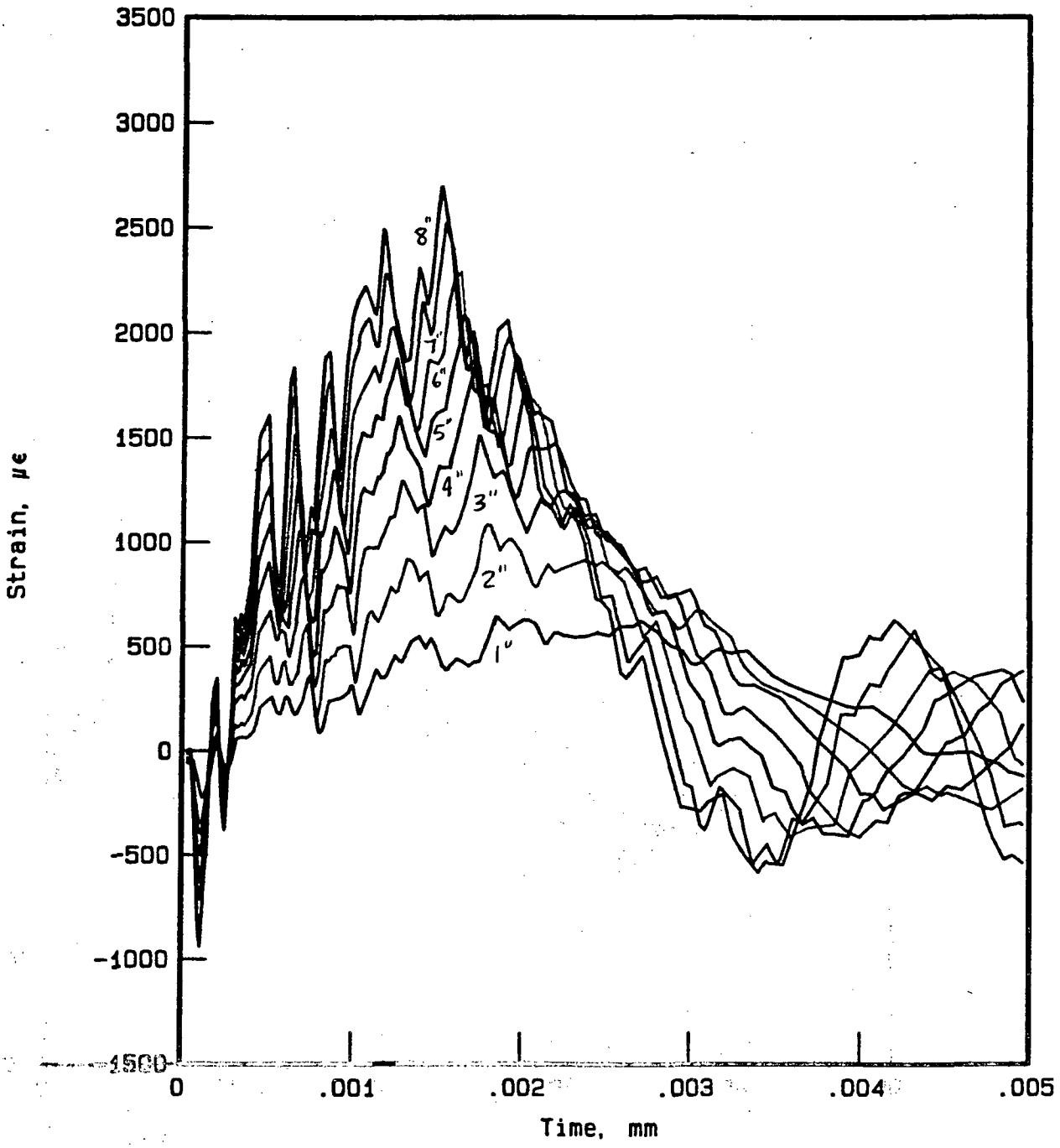

Low-Velocity Impact Test on 5" Length Beam
Specimen A-D-B
Strain B

Fig. 15-B

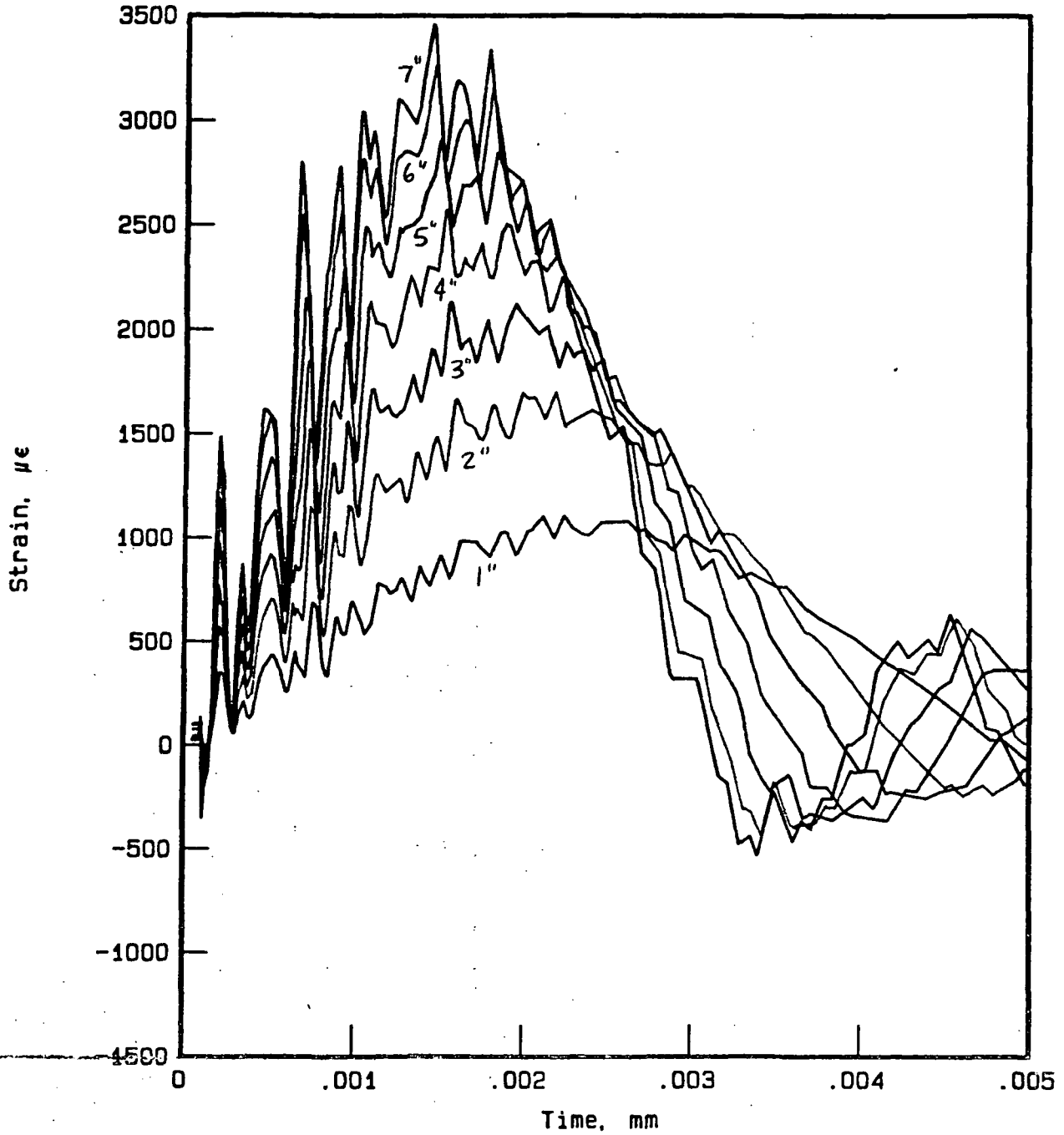

Low-Velocity Impact Test on 5" Length Beam
Specimen A-D-B
Strain C

Fig. 15-C

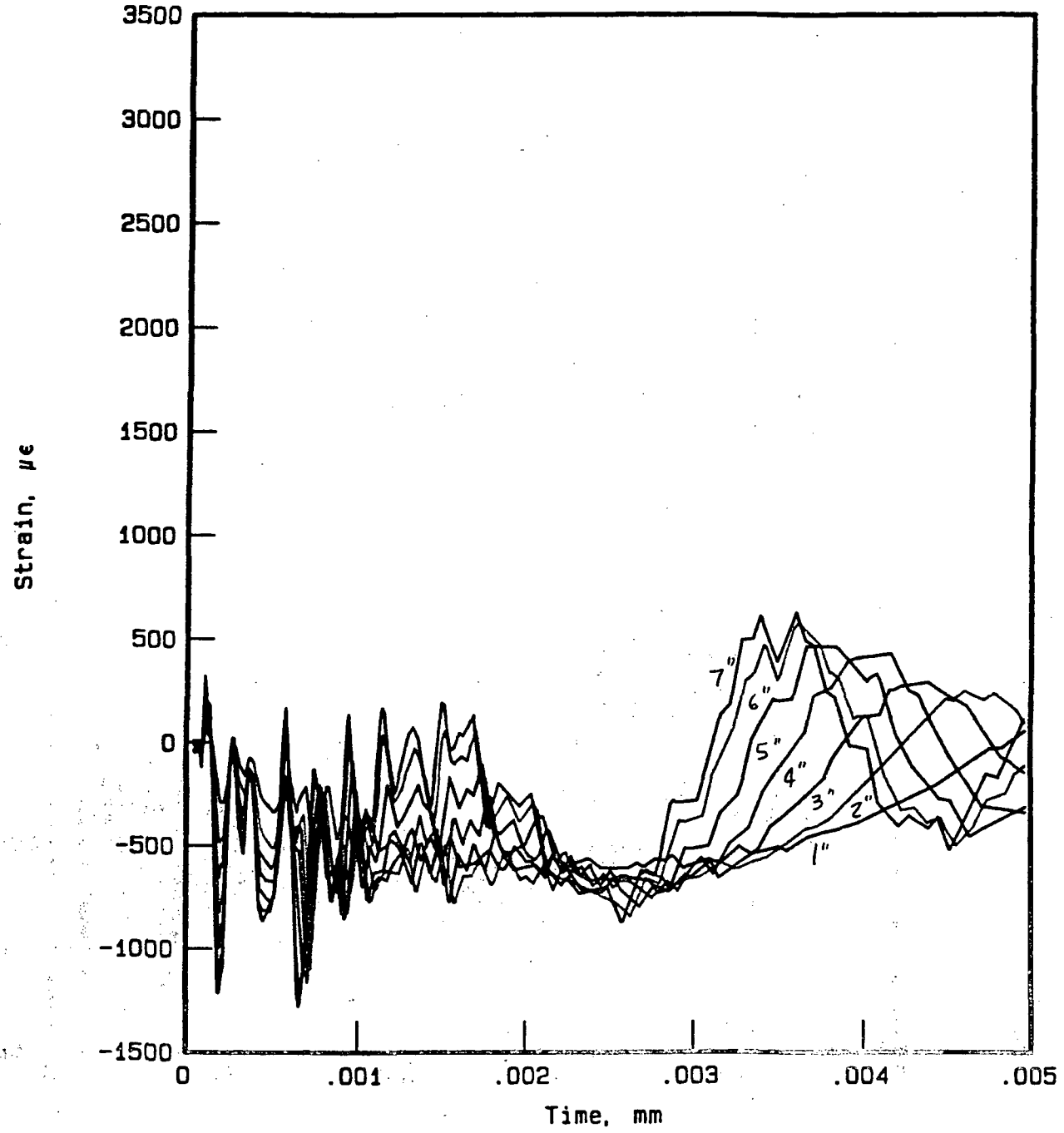

Low-Velocity Impact Test on 5" Length Beam
Specimen A-D-B
Strain D

Fig. 15-D

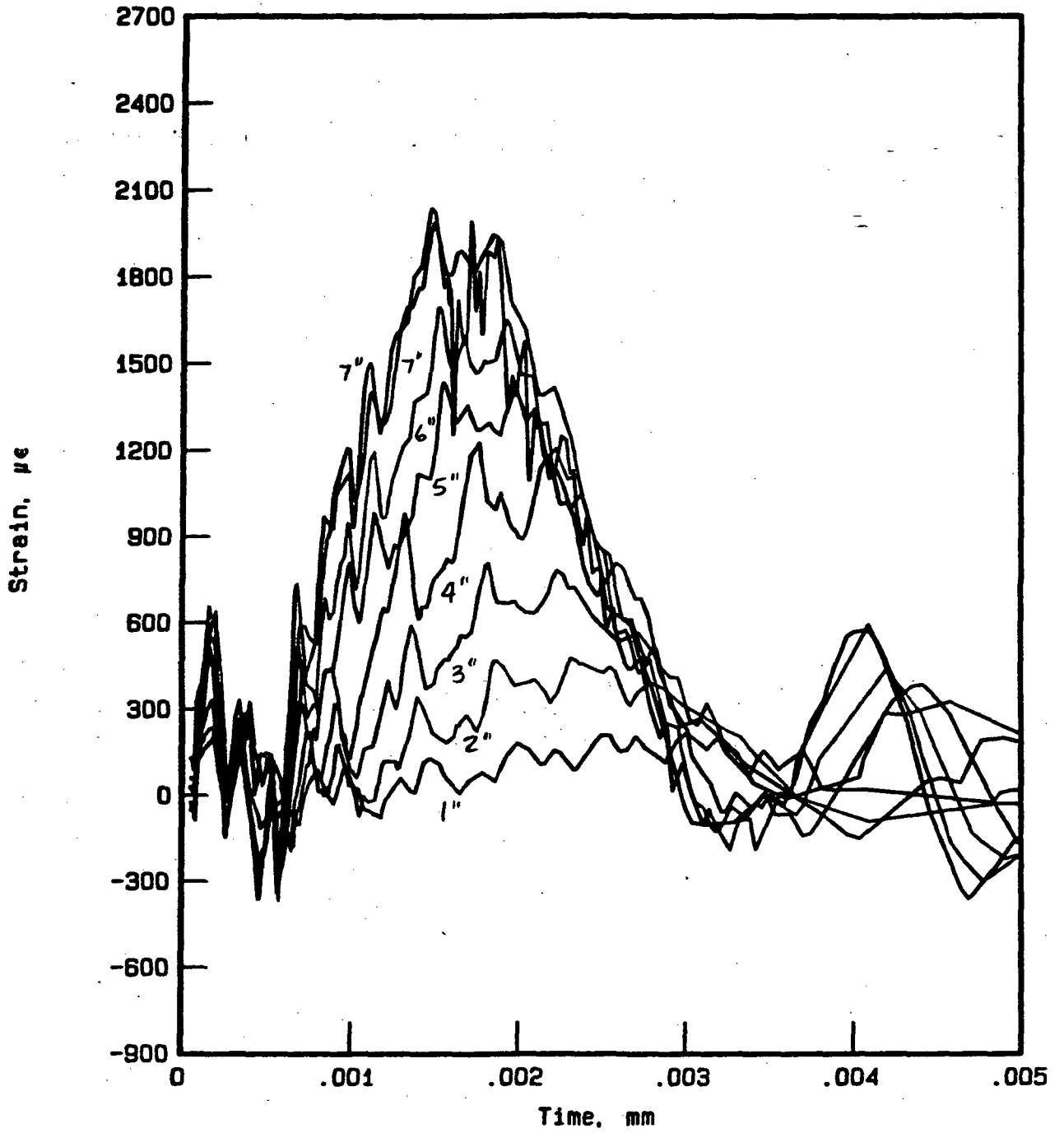

Low-Velocity Impact Test on 5" Length Beam
Specimen B-D-B
Strain A

Fig. 16-A

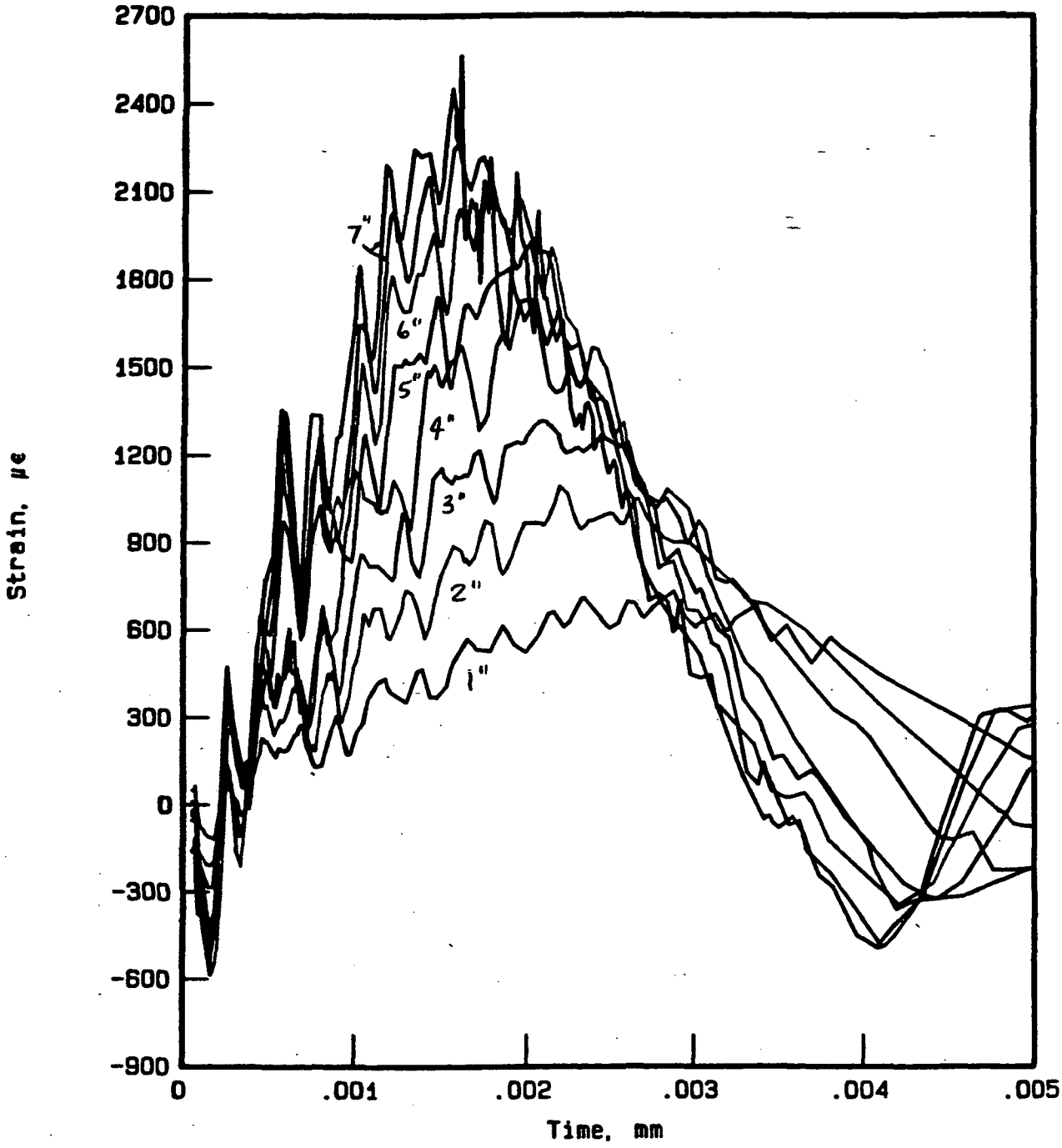

Low-Velocity Impact Test on 5" Length Beam
Specimen B-D-B
Strain B

Fig. 16-B

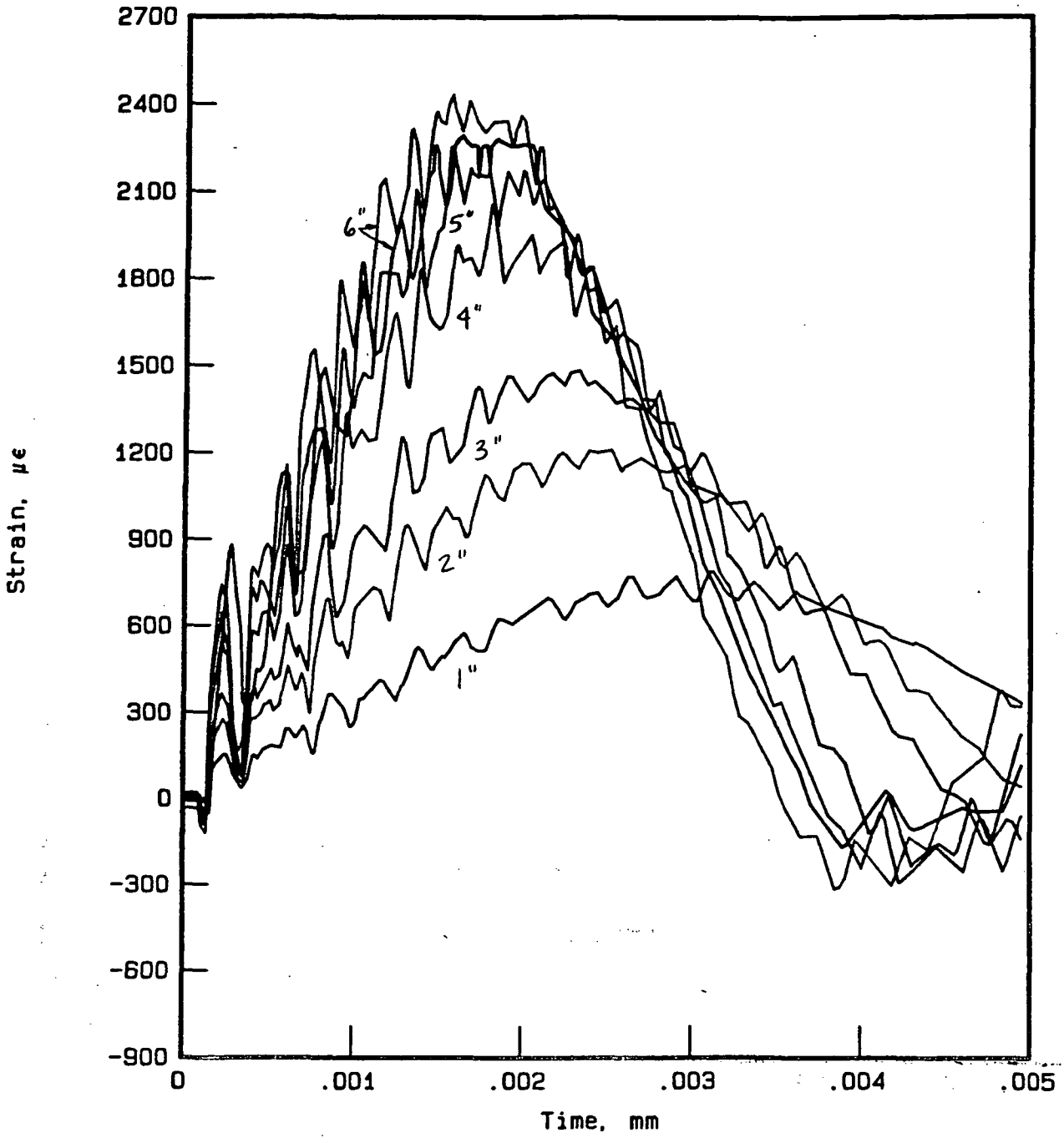

Low-Velocity Impact Test on 5" Length Beam
Specimen B-D-B
Strain C

Fig. 16-C

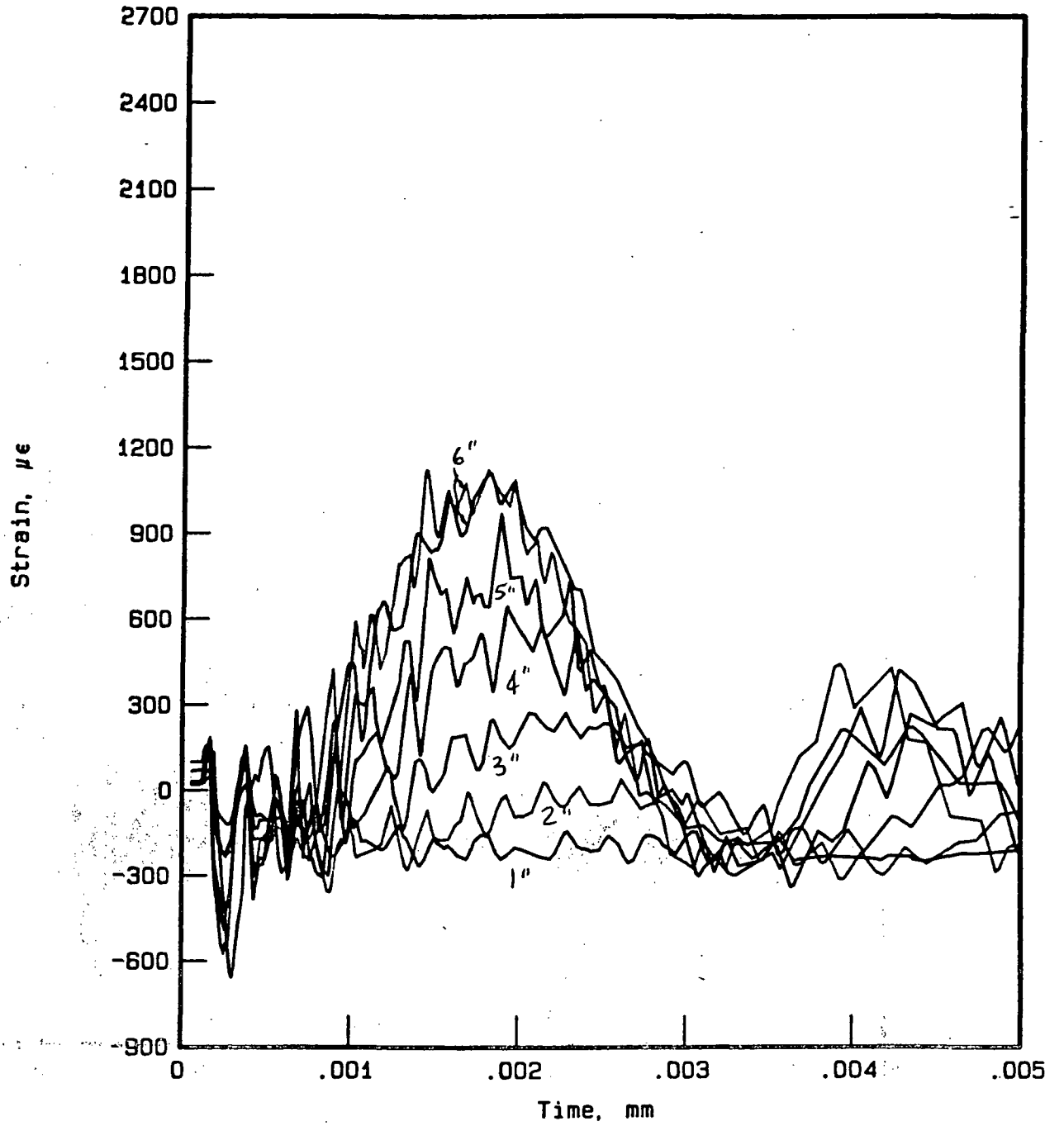

Low-Velocity Impact Test on 5" Length Beam
Specimen B-D-B
Strain D

Fig. 16-D

TABLE 1

	Material A	Material B
Description	woven fabric laminate	tape laminate
Plate thickness	1.64 mm	1.04 mm
$E_{flexural}$	37.9 GPa	53.1 GPa
E_{SHEAR}		2.5 GPa
Indentation Constant	46 MN/m	39 MN/m
Poisson's ratio	0.3	0.3
Radius of plate	63.5 mm	63.5 mm

Low-Velocity Impactor
constants used in analysis

M - mass of ball and cantilever =

K - stiffness constant for cantilever =

	Coefficient	95 % Confidence Interval Lower Limit	Upper Limit
Constant	3.8278903E+00	3.7973384E+00	3.8584422E+00
X^1	1.3583412E+00	1.3436359E+00	1.3730464E+00

A

$y = e^{3.83} x^{1.36}$

$y = 46.0\ x^{1.4}$ KN/mm

$y = 46000$ KN/m $= 46$ MN/m